DESIGN AND ANALYSIS OF FIXTURING METHODS FOR MESOSCALE MANUFACTURING

By

KOUSTUBH J. RAO

A THESIS PRESENTED TO THE GRADUATE SCHOOL
OF THE UNIVERSITY OF FLORIDA IN PARTIAL FULFILLMENT
OF THE REQUIREMENTS FOR THE DEGREE OF
MASTER OF SCIENCE

UNIVERSITY OF FLORIDA

2009

To my parents and my sister
Thank you for always being there for me

ACKNOWLEDGMENTS

I thank my advisor, Dr. Gloria Wiens, Associate Professor, Department of Mechanical and Aerospace Engineering, University of Florida, for her continuous support and guidance. I would also like to thank my committee members Dr. Hitomi Yamaguchi Greenslet, Associate Professor, and Prof. John Schueller, Professor.

I express my deep sense of gratitude to my family members for their perennial moral support and encouragement. I also record my special thanks to my friends and lab mates (Space, Automation and Manufacturing Mechanisms Laboratory and Space Systems Group) for making my stay at UF very memorable.

TABLE OF CONTENTS

page

LIST OF TABLES

LIST OF FIGURES

LIST OF ABBREVIATIONS

mMTs	mesoscale Machine Tools
FIXEL	Fixture Element
PKM	Parallel Kinematic Mechanism
PRBM	Pseudo Rigid Body Model
TIR	Total Indicated Reading

Abstract of Thesis Presented to the Graduate School
of the University of Florida in Partial Fulfillment of the
Requirements for the Degree of Master of Science

DESIGN AND ANALYSIS OF FIXTURING METHODS FOR MESOSCALE MANUFACTURING

By

Koustubh J. Rao

August 2009

Chair: Gloria Wiens
Major: Mechanical Engineering

The workpiece-fixture and the tool-workpiece interactions are important factors for a manufacturing process and play a major role in the efficacy of the process. They lead to non-beneficial machine performance in terms of inaccurate dimensioning and improper finishing of the workpiece. These interactions become even more important for mesoscale manufacturing because of the higher accuracy requirements. In addition, the type of fixturing used on mesoscale machine tool system sets a limit on the ability to achieve high accuracy of dimensions. Fixturing also remains a critical issue impeding the integration and autonomous operation of micro/mesoscale manufacturing systems. To push beyond these accuracy limits, innovative work-holding approaches are needed. This study presents an investigation of four fixture element (fixel) designs for fixturing to be incorporated into mesoscale manufacturing systems. These fixels help in improving the process accuracy by taking into account the effects of tool runout. Using compliant mechanisms and components (e.g., monolithic four-bar mechanisms and/or cantilever beams), fixels exhibiting mechanically adjustable stiffness characteristics are achievable. Manually or automating the stiffness adjustments, these fixels provide a functionality for enabling greater control of the response of the workpiece due to runout and variation in contact forces at the tool-workpiece-fixture interface. The method of implementing these fixel

designs (using four fixels) for common manufacturing operations is suggested in addition to the designs. Each design has specific mechanical parameters for its fixels and adjustable stiffness characteristics are achieved by varying these parameters. The monolithic four bar design has two mechanical variables whereas the three cantilever/compliant beam fixel designs require actuation of only one mechanical parameter. To quantify the fixel functionality and its dynamic range, the theoretical models of the stiffness characteristics expressed as a function of these mechanical variables are presented for each of the designs. Upon establishing a common stiffness range for the three compliant beam fixel designs, a metric is formed for better comparison between the designs. This metric is based on the sensitivity of stiffness expressed as a function of slenderness ratio and an operation range, bounded by a minimum possible stiffness value shared by the cantilever beam fixture models. The slenderness ratio is defined as the ratio of the minimum length of the cantilever beam to its maximum width while the operation range is determined by the ratio of the minimum and maximum possible values of the fixel's mechanical variable. Using this metric, results are generated for each of the designs and then compared with one another to highlight the advantages and disadvantages of each design. Models for one of the fixel designs are then developed to perform dynamic analysis and understand the behavior of the fixturing design under manufacturing operation conditions.

CHAPTER 1
INTRODUCTION

1.1 Background

The growing trend towards miniaturization has impacted technologies in virtually every field, from medicine to manufacturing. Consequently, a dramatic shift is occurring within the manufacturing paradigm toward the development of complementary capabilities for producing miniaturized products. Furthermore, this shift has led to research efforts on micro/meso levels, bridging the gap between the micro and macro worlds. The creation of mesoscale machine tools (mMTs) that are less expensive and more portable than conventional precision machine tools is an indication to these efforts.

However, mesoscale manufacturing is still faced with critical issues in accuracy due to the adverse affects resulting from tool-workpiece and the workpiece-fixture interactions. These inaccuracies could be due to runout in the tool, misalignment of the tool/workpiece, workpiece material properties, etc. These challenges are magnified for the complicated process of creation of micron features on micro and macro-sized parts, where fixturing and material handling pose a problem. This is an area with significant importance, yet there has been limited research on addressing these problems. The objective of this study is to contribute towards research on mesoscale manufacturing by introducing fixturing designs which can facilitate controlling the tool-workpiece interface dynamics.

1.2 Motivation

In prior research related to mesoscale manufacturing, designs for reconfigurable manipulators consisting of compliant elements and actuators for part positioning and handling have been developed. These methods and devices typically manipulate components that are adhered to the device or a base material and do not have the ability to directly control the tool-

workpiece interactions. By developing fixturing devices which have the ability to passively or actively control these interactions, the repeatability and precision of mesoscale machine tools can be enhanced. In the context of controlling the tool-workpiece interface dynamics, mechanical adaptability is a key factor and can be of advantage to the current situation. The feasibility of mechanical adaptability at the mesoscale and macro-scale for fixturing has been successfully demonstrated but has not been implemented. For the work reported in this thesis, the premise of the active fixturing can be stated as follows. If fixturing methods which are capable of providing stiffness adjustments are developed, they will enable greater control of the response of the workpiece due to runout and variation in contact forces at the tool-workpiece-fixture interface.

Consequently, it is necessary to develop designs and methods of implementation for mechanically adaptable fixturing devices comprising of fixels (fixture elements). Such a fixturing system is illustrated in Figures 1-1 and 1-2, consisting of four fixels and integrated with a mesoscale machine tool. In the system illustrated in Figure 1-1, the fixels are in a horizontal plane whereas the plane of application of the fixture designs shown in Figure 1-2 is in the vertical plane. In such a system, gravitational effects will also play a major role. Once fixel designs are developed, a method to compare them would be required along with the analysis of the designs to validate them.

1.3 Focus of Research

This thesis focuses on designs for fixels for passive/active fixturing which can provide mechanically adjustable characteristics. In this thesis four candidate designs are presented for fixturing mesoscale workpieces. The first design consists of monolithic compliant four-bar mechanism type fixels. The other three fixturing designs consist of cantilever beam type fixels. These designs must be evaluated in their ability to control stiffness, both in range and direction, via a minimal set of mechanical adjustments. To quantify the fixel functionality and its stiffness

range, this study presents the theoretical models for determining the stiffness characteristics at the point of fixel-workpiece contact. These stiffness characteristics are expressed as functions of the mechanical variables of each of the fixel designs. Through variable stiffness characteristics, the response of the workpiece due to runout and variation in contact forces at the tool-workpiece-fixture interface can then be better controlled. In order to determine the capabilities of these fixturing methods, the modeling and analysis of candidate fixel designs is done.

The stiffness adjustability of each of such fixels can be integrated in a coordinated manner with other (adjustable) fixels. The fixturing system formed by combining these independent fixels with the workpiece takes the form of a parallel kinematic mechanism (PKM). In this PKM setup, the fixels act as the independent kinematic chains and the workpiece is the end-effector, thus forming a closed loop system. Leveraging these similarities with the PKM, passive/active fixturing also has the potential of providing a dual-capability of fixturing as well as manipulating micro/mesoscale workpieces [8], [9]. Furthermore, via stiffness adjustments of the fixels, the fixturing device will have the ability to tune the kinematics and dynamics of the mesoscale machine tool and control the tool-workpiece interface dynamics. These characteristics can be used to reduce the errors caused by tool runout to improve the accuracy of the process and reduce the effects on the tool properties. This stiffness relationship can then be applied towards development of efficient control algorithms implemented through actuated adjustments of the mechanical variables of the fixels.

While this thesis focuses on the mMT application, it should be noted that the methodology presented herein is applicable to both macro and mesoscale manufacturing. Furthermore, mesoscale manufacturing is performed using various machine tool sizes that vary from small to medium sized desk top machine tools to the more traditional sized machine tool.

1.4 Literature Review

As mentioned in the previous section, there has been an increase in the research on developing more efficient and accurate mesoscale machine tools (mMTs). Some of the mMTs that have been developed or are being developed are less expensive and more portable than conventional precision machine tools. This is achieved by developing a thorough study of the dynamic behavior of the mMT [1], developing different methods for their calibration [2] and evaluation of the performance of the developed systems in mesoscale processes.

There has been prior research done on better understanding the process parameters that have a large effect on a mMT system and estimating the optimal operation conditions for such systems. The parameters such as depth of cut, magnitude of cutting forces, feed rate and spindle rotation speed impact the performance of a mMT system. The spindle speed is usually high for such systems and is in the order of 60000 rpm (with certain processes reaching speeds up to 120000 rpm) while the cutting forces are usually in the order of 10 mN [3]. Any design of a mesoscale system or its components should be developed and analyzed for these values of the parameters.

In recent years, research is being carried out on using compliant mechanisms for developing positioners for mesoscale systems which assist part positioning by reducing the alignment errors. Culpepper and Kim [6] developed a six-axis reconfigurable manipulator consisting of compliant elements and actuators for part positioning. The characteristics of compliant mechanisms can then be extended to not just positioners, but also to fixturing systems. Since the feasibility of mechanical adaptability at the mesoscale [4], [5] and macro-scale [7] for fixturing has been already been successfully demonstrated (without implementation), research needs to be done to take advantage of these properties. The use of compliant mechanisms to achieve variable stiffness characteristics can therefore improve the performance of mMTs.

The performance of a mMT is dependent on many process factors such as the spindle rotation speed, the runout in the tool, feed rate, cutting force and the depth of cut. Tool runout is one of the important parameters which directly affects the accuracy of the mesoscale manufacturing process [3]. Runout, often measured as Total Indicated Reading (TIR), is defined as the difference between the maximum and the minimum distance of the tool point from the axis of rotation measured over one revolution as illustrated in Figure 1-3 [12]. Radial runout is the result of a lateral (parallel) offset between the rotational axis of the tool and the central axis of the collet/spindle system. Runout can also occur due to variation in the length of the teeth of the cutter resulting in varying depth of cut. A longer tooth will have a deeper cut as compared to the teeth of the correct size, thus affecting the accuracy of the machining process. The runout from the spindle of the system (or from varying teeth dimensions) causes an extraneous force on the workpiece and results in increased excitations [3]. Even though there exists a relationship between runout and the resulting contact force, researchers have yet to define the specifics of this relationship in terms of magnitude, frequency and amplitude as a function of the runout and tool-workpiece material properties. Non-contact precision capacitance sensors are typically used to dynamically measure the runout of a tool. These sensors use capacitance technology to measure the runout and provide accurate readings for frequencies up to 120,000 rpm.

There are many factors which affect the tool runout such as frequency of spindle rotation, the duration of the operation and the tool-workpiece interactions. The runout value increases for higher frequencies and these values change depending on the precision of the setup. The typical values of runouts for high precision systems are in the range of 0.001 mm to 0.006 mm and in the range of 0.03 mm to 0.05 mm for lower precision systems [12]. Although considerable research is being carried out to achieve reduced runout, it still remains a challenge. Hence,

alternate approaches are required to achieve control on the adverse affects of tool runout. Using fixturing methods with variable stiffness characteristics is one such approach.

1.5 Thesis Outline

This thesis is organized in the following manner. After giving a brief introduction to the growing trend towards micro/mesoscale manufacturing and the challenges faced in accuracy due to the adverse affects resulting from tool-workpiece interactions in Chapter 1, Chapter 2 summarizes the problem statement followed by a discussion of the assumptions made in developing the fixel designs. This is followed by Chapter 3 which provides a detailed description of the principles of each of the four fixel designs and the relationships between fixel stiffness and the specific design parameters. Chapter 4 describes the metric obtained to compare the compliant beam fixel designs followed by the plots depicting the stiffness characteristics of the fixel designs. Chapter 5 deals with the implementation and analysis of one of the fixel designs in a mesoscale manufacturing process under typical operation conditions. Later Chapter 6 identifies the major conclusions and highlights areas where this work needs to be further developed.

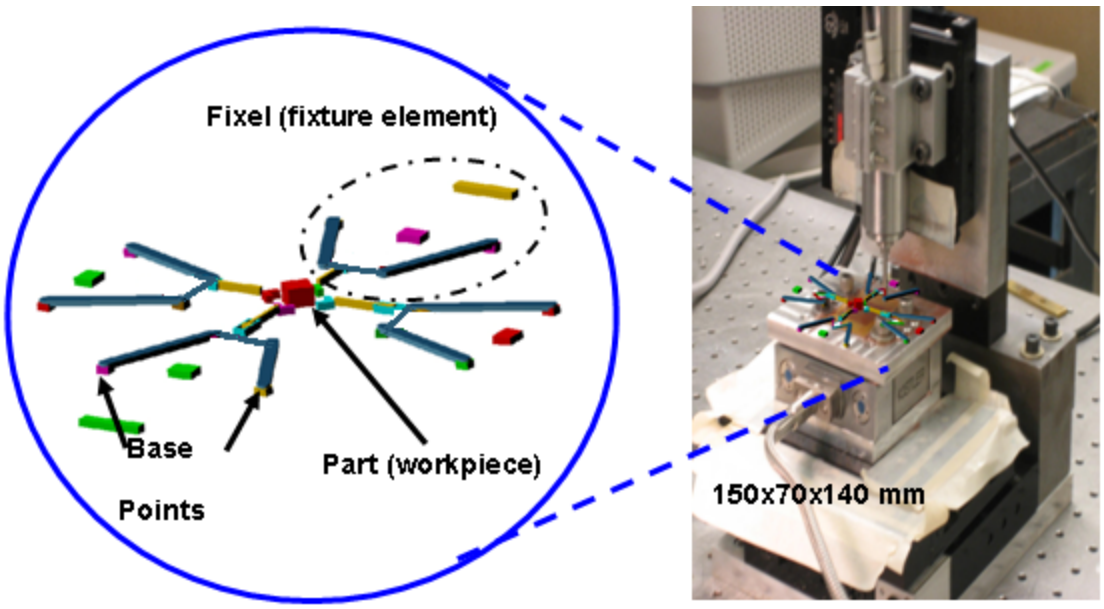

Figure 1-1. Conceptual Integration of Fixturing and Mesoscale Machine Tool (horizontal plane of application) (mMT stage courtesy of J. Ni at S.M. Wu Manufacturing Research Center, University of Michigan, Ann Arbor, MI)

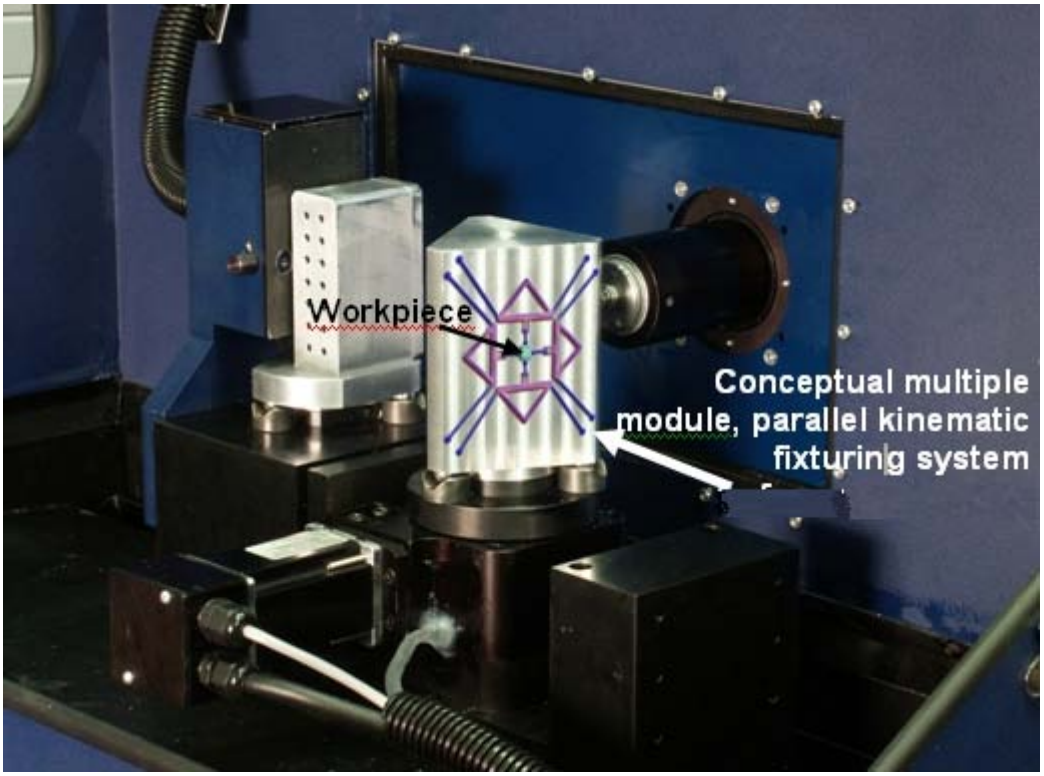

Figure 1-2. Conceptual Integration of Fixturing and Mesoscale Machine Tool (vertical plane of application). (mMT stage courtesy of Thomas N. Lindem at Atometric, Inc., Rockford, IL)

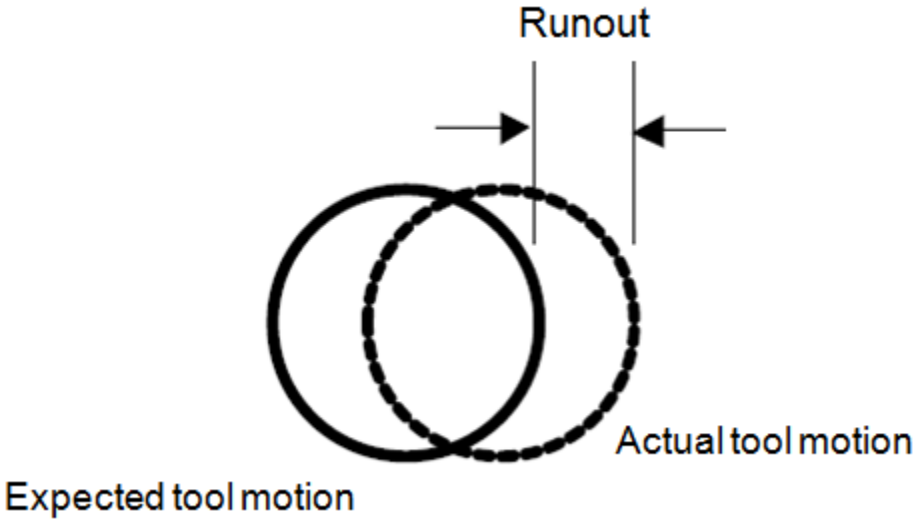

Figure 1-3. Illustration of runout error

CHAPTER 2
THEORETICAL FIXEL MODEL ASSUMPTIONS

As stated in Chapter 1, the overall objective of this thesis is to characterize the functionality and capabilities of an active fixturing methodology for mesoscale manufacturing. This requires a clear understanding of the compliant nature of each fixel and the system of fixels as well as the dynamic impact of active fixturing on the tool-workpiece interface dynamics. Chapter 1 first provides a description of the active system and how it may be implemented on two different typical micro/mesoscale machine tools (vertical and horizontal planes of application). This is followed by a narrowing of the problem statement to fixel design development, modeling and analysis in terms of fixel stiffness and dynamics. In this thesis, the workpiece-tool interface scenario used as a basis for analysis and demonstration is tool runout and its adverse effects on feature dimensional accuracy.

2.1 Problem Statement

The focus of the current study is to develop fixture designs which have variable stiffness characteristics and can be implemented on typical mesoscale machine tool systems. After developing the designs, modeling and analysis is to be performed to validate the implementation of the design in a typical mMT setup. Four different fixel designs are considered in this study, a compliant four-bar mechanism type fixel and three beam type fixels with the beam type fixels being fundamentally similar.

2.2 Assumptions

While the four bar mechanism based fixel design consists of compliant components and will typically be fabricated as a monolithic compliant structure, the modeling of this design is done using its Pseudo-Rigid Body Model (PRBM). Therefore, the assumption for the compliant four bar mechanism is a four bar mechanism consisting of rigid links with spring loaded joints.

Comparatively, there are different methods for obtaining the compliant structure. One method is to locate all the compliance within joint centric locations of the device for which the lengths of the rigid segments are large relative to the lengths of the flexural members. The flexure members provide localized compliance analogous to a spring loaded kinematic joint. Another method is to have a structure with a kinematic topology that yields motion under loading analogous to a four bar mechanism. Either of these methods can be modeled using the PRBM method yielding kinematically and dynamically equivalent designs. In this thesis, the first method is assumed (details of which can be found in a later section 3.1.2). It should however be noted that the second method is anticipated the preferred method for yielding the designs to be fabricated and implemented in the commercial application. This will be the subject of future research and development.

For the beam type fixels, three different implementation approaches are explored. The fundamentals of the beam type designs arrive from solid mechanics principles for beam deflections. As known from these fundamentals, the beam deflections can be expressed as a function of a given load and support locations [10]. From these principles, the fixel's stiffness (proportional to Δforce over Δdisplacement at the point of fixel-workpiece contact) can be quantified for each fixel configuration. The Euler-Bernoulli beam theory assumption is made in deriving the theoretical models, i.e., the length of the fixel beam element (denoted by L) is constrained to be at least 10 times larger than its cross-sectional thickness (denoted as width h herein) as shown in Equation 2-1.

$$L / h \geq 10 \tag{2-1}$$

This ratio of L to h is an important parameter for the designs which is explained in the later sections.

CHAPTER 3
PRINCIPLES OF THE DESIGNS

The principles involved in each of the four fixture designs proposed in this study and the mechanical parameters involved in each of the designs are described in this chapter. The relationship between these parameters and the fixel stiffness is then established followed by developing the variable stiffness characteristics of the designs.

3.1 Design 1

The first fixture design under consideration is one in which each fixel is a monolithic compliant four-bar mechanism consisting of links and compliant flexure joints as illustrated in Figure 3-1. The length of the links and the length of the flexural joints are the characteristics of this design. To simplify the modeling, an equivalent pseudo-rigid-body model (PRBM) of this fixel is developed in this study. The next section gives a brief introduction to compliant mechanisms and the development of equivalent PRBMs.

3.1.1 Introduction to Compliant Mechanisms

Compliant mechanisms are mechanisms which transfer motion, an input force or energy from one point to another, using flexible members. Unlike rigid body mechanisms, where the mobility of the mechanism is achieved through the degree of freedom in joints (kinematic pairs), compliant mechanisms achieve mobility through the elastic deformation of the flexible members. An example of a compliant crimping mechanism similar to a vice grip is shown in Figure 3-2. This mechanism consists of three flexible members, unlike in a vice grip which consists of revolute joints instead of these flexural pivots. The input force applied on the hand grips results in some energy being stored in the mechanism in the form of strain energy in the flexural pivots. Some examples of other common compliant devices are binder clips, backpack latches, paper clips, etc.

The two main advantages of compliant mechanisms are cost reduction and increased performance [11]. Since compliant mechanisms are mostly monolithic and do not require kinematic pair type joints or pins, this results in reduced part count as compared to a rigid body mechanism. This directly results in reduction in assembly time, improved manufacturing process reliability and the ability to be easily miniaturized. Since there is no relative sliding motion between the surfaces of the joints as seen in rigid body mechanisms, friction is generally assumed negligible in compliant devices. This results in reduced wear and thus reduced maintenance in terms of lubrication. Such mechanisms also do not have the inherent problems of backlash and/or joint tolerances which is common in jointed mechanisms. Thus, these mechanisms also exhibit increased precision and increased reliability.

3.1.2 Pseudo Rigid Body Model of a Compliant Mechanism

Although there are numerous advantages of compliant mechanisms, there are some challenges faced with respect to analyzing and designing them. The most well known technique to design and analyze compliant systems that undergo large deflections is the use of Pseudo Rigid Body Model (PRBM). In this concept, the deflection of flexible members is modeled using equivalent rigid body components. The flexural pivots are modeled as kinematic pair type joints/pins with the stiffness of the flexural members represented by torsional springs within the joints. For each PRBM, the most important consideration is the placement of the revolute/pin joints and the value of the spring constant to be assigned [11].

A monolithic compliant four bar mechanism consists of four rigid links connected by flexural pivots. A PRBM for such a mechanism is modeled by placing revolute joints at the center of the flexible segments and torsional springs at each of these joints. The placement of the joints is based on the assumption that the lengths of the flexural members are small relative to the lengths of the rigid segments.

3.1.3 PRBM of the Fixel

Figure 3-3 presents the pseudo-rigid-body model of the four-bar mechanism type fixel developed as explained in the previous section. Each of these four bar fixels will provide directional variable stiffness characteristics to the workpiece fixturing setup within its plane of motion. In this model, the joint flexural pivots are modeled as revolute joints (2, 3, 4 and 6) as shown in the figure. The stiffness of the flexural pivots is expressed by adding torsional springs of spring constants k_2, k_3, k_4 and k_6, respectively. The base link has a length of L_1 while the rigid links have equivalent constant link lengths of L_2, L_3, L_4, and L_5, and the contact point of the fixel with the workpiece occurs at the end of link L_5 which acts as the interface element. The angles between the links L_1 and L_2 is labeled as θ_2 (called the base angle), the angle between L_1 and L_4 as θ_4, the angle between L_2 and L_3 as θ_3, the angle between L_3 and L_4 as θ_6 and the angle made by link L_5 with the vertical is denoted as θ_5. Due to the geometry of the four bar model, the values of the angles θ_3, θ_4, θ_5 *and* θ_6 are functions of θ_2 and the link lengths and hence, can be obtained for any configuration of the model. These relationships are expressed using the Equations 3-1.

$$
\begin{aligned}
d_{36} &= sqrt(L_1^2 + L_2^2 - 2L_1L_2\cos\theta_2) \\
\theta_{3a} &= \sin^{-1}(L_1\sin\theta_2 / d_{36}) \\
\theta_{3b} &= \cos^{-1}((L_3^2 + {d_{36}}^2 - L_4^2) / 2L_3d_{36}) \\
\theta_3 &= \theta_{3a} + \theta_{3b} \\
\theta_4 &= \sin^{-1}(d_{36}\sin\theta_{3b} / L_4) \\
\theta_6 &= 2\pi - \theta_2 - \theta_3 - \theta_4 \\
\theta_5 &= -\pi + \theta_2 + \theta_3
\end{aligned}
\qquad (3\text{-}1)
$$

As mentioned previously, the tip of the interface element (link L_5) is in contact with the workpiece. The x and y coordinates (x_c, y_c) of this point contact with respect to the X, Y frame affixed to the base link are given by Equations 3-2. Hence, the change in y_c in one configuration

to another configuration represents the displacement of the point of contact which will be required to calculate the (vertical) stiffness constant at the point of contact.

$$x_c = -1/2L_1 + L_2\cos\theta_2 + (1/2)L_3\cos\theta_5 - L_5\sin\theta_5$$

$$y_c = L_2\sin\theta_2 + (1/2)L_3\sin\theta_5 + L_5\cos\theta_5 \quad (3\text{-}2)$$

For this design, the stiffness characteristics of each fixel as seen at the point of fixel-workpiece contact is mechanically adjusted by extending the base length (L_1) and/or an input angle (θ_2). Hence, L_1 and θ_2 represent the mechanical parameters for this design with the stiffness constant being a function of these parameters.

3.1.4 Derivation of Stiffness of the Fixel at Contact Point (Along y-direction)

To derive the stiffness values for the PRBM, the link lengths were chosen such that L_2=L_4 and L_3 is shorter than the other links. Also, all flexures (torsional springs) are assumed to have equal stiffness values. During the equilibrium configuration of the fixel, there is no net force acting on the contact point and hence, the joint flexure's torsional loads are calculated using angles measured from this unloaded equilibrium. At this equilibrium configuration, all the link lengths and the respective angles are at their initial values and the link L_3 is horizontal. At this configuration, the length of base link is denoted as L_{1o} and θ_2 is denoted as θ_{2o} as shown in Figure 3-4a (the remaining angles are also denoted with similar subscripts). When one or both of the mechanical parameters of the design (L_1 and θ_2) are varied from their equilibrium values, assuming contact is not lost, it results in a contact force (F_c) acting at the workpiece-fixture interface and a corresponding change in the y-coordinate of the point of contact (y_c). When the base length and/or the base angle are again changed, it results in a corresponding change in F_c and y_c (denoted by ΔF_c and Δy_c) as compared to the previous configuration. The ratio of this change in contact force to the change in the position of the point of contact is defined as the

stiffness of the fixel at the point of contact. Hence, to derive the stiffness value, the corresponding values of ΔF_c and Δy_c are calculated. The procedure to calculate this stiffness is described next.

The base link length and the base angle can each be varied within particular kinematic ranges with the initial value of the base length operation range being L_{1o}. The range of values for base length can be chosen according to the footprint of the setup. To calculate the range of values of the base angle, a particular value of base length is chosen from the range and the unloaded equilibrium configuration for this value (as shown in Figure 3-4a) is first determined. Each of these unloaded equilibrium configurations, result in a four-bar mechanism and the two toggle positions (motion limits) for this four bar model are then determined. These limits provide the corresponding kinematic range of base angles that comply with the design at that particular base length. This process is repeated for all possible values of the base length and the individual range of values of base angles is obtained for all the base lengths. From these different sets of ranges of base angles, the values which are common to all the sets represent the final operation range for the input base angle θ_2.

To calculate stiffness, the base length is first changed to a particular value in the operation range (say L_1) using a prismatic actuator shown in Figure 3-3. Due to the geometry of the four bar model, this change in the base length results in the base angle changing from θ_{2o} to $\theta_{2_0}^{'}$ as shown in Figure 3-4b (with the remaining angles similarly changing to θ_{3o}', θ_{4o}' *and* θ_{6o}'). Then, the base angle is increased to a certain value (say θ_{2i}) within the operation range using the revolute joint actuator shown in Figure 3-3. This increment of $\Delta\theta$ will result in a change in the angles of the model (i.e. change in θ_{3i}, θ_{4i} and θ_{6i}) along with a displacement of the link L_5 and a contact force (say F_{ci}) acting on the link L_5. The contact force occurs on the link L_5 so that the

model remains in static equilibrium. The configuration of the fixel at this instant is shown in Figure 3-4c.

At this configuration, a static force analysis is carried out on the model and the equation shown in Equation 3-3 is obtained.

$$\begin{bmatrix} F_{C_{xi}} \\ F_{C_{yi}} \\ F_{32_{xi}} \\ F_{32_{yi}} \\ F_{34_{xi}} \\ F_{34_{yi}} \end{bmatrix} = \begin{bmatrix} 1 & 0 & 0 & 0 & 0 & 0 \\ 1 & 0 & 1 & 0 & 1 & 0 \\ 0 & 1 & 0 & 1 & 0 & 1 \\ 0 & 0 & M_{4,3} & M_{4,4} & 0 & 0 \\ M_{5,1} & M_{5,2} & M_{5,3} & M_{5,4} & M_{5,5} & M_{5,6} \\ 0 & 0 & 0 & 0 & M_{6,5} & M_{6,6} \end{bmatrix}^{-1} \begin{bmatrix} 0 \\ 0 \\ 0 \\ V_4 \\ V_5 \\ V_6 \end{bmatrix} \tag{3-3}$$

where F_{lm} is the force acting on link l by link m, subscripts x and y indicate the corresponding (x,y) components of the forces F_{lm} and the subscript i denotes the current configuration. In addition, the values of V_4, V_5, and V_6 for the corresponding torsional springs are obtained using the value of the spring constant and the change in angle at the particular joint as shown in Equation 3-4. The elements of the inverse matrix in Equation 3-3 are functions of the link lengths and the angles and are given by Equation 3-5.

$$\begin{aligned} V_4 &= -\left[\left(k_2 * \left(\theta'_{2_0} - \theta_{2i}\right)\right) + \left(k_3 * \left(\theta_{3i} - \theta'_{3_0}\right)\right)\right] \\ V_5 &= \left(k_3 * \left(\theta_{3i} - \theta'_{3_0}\right)\right) + \left(k_6 * \left(\theta'_{6_0} - \theta_{6i}\right)\right) \\ V_6 &= -\left[\left(k_6 * \left(\theta'_{6_0} - \theta_{6i}\right)\right) + \left(k_4 * \left(\theta_{4i} - \theta'_{4_0}\right)\right)\right] \end{aligned} \tag{3-4}$$

$$
\begin{aligned}
M_{4,3} &= L_2 * \sin(\theta_{2i}) & M_{4,4} &= -L_2 * \cos(\theta_{2i}) \\
M_{5,1} &= -L_5 * \cos(\theta_{5i}) & M_{5,2} &= -L_5 * \sin(\theta_{5i}) \\
M_{5,3} &= \frac{L_3}{2} * \sin(\theta_{5i}) & M_{5,4} &= -\frac{L_3}{2} * \cos(\theta_{5i}) \\
M_{5,5} &= -\frac{L_3}{2} * \sin(\theta_{5i}) & M_{5,6} &= \frac{L_3}{2} * \cos(\theta_{5i}) \\
M_{6,5} &= L_4 * \sin(\theta_{4i}) & M_{6,6} &= L_4 * \cos(\theta_{4i})
\end{aligned}
\qquad (3\text{-}5)
$$

Using the above equations, the value of the contact force at the current configuration ($F_{C_{yi}}$) is calculated. The value of y-coordinate at this instant (y_{C_i}) is then calculated using the expression for y_c shown in Equation 3-2 and the current values of the angles.

Keeping the base length fixed, the base angle is then incremented to another value (say $\theta_{2_{i+1}}$ within the kinematic range) which results in a corresponding change in the remaining angles. The new configuration of the model at this instant is shown in Figure 3-4d. A static force analysis is again conducted on the model in this configuration and equations similar to Equations 3-3 to 3-5 are obtained. Using these equations, the value of the contact force at the new configuration ($F_{C_{y_{i+1}}}$) and the value of y-coordinate at this new configuration ($y_{C_{i+1}}$) are then calculated. The difference in the contact forces at the new configuration and the previous configuration is calculated and is denoted by $(\Delta F_c)_{i+1}$ followed by calculating the displacement of the point of contact, $(\Delta y_c)_{i+1}$ (difference in the y-coordinates of the two configurations). The ratio of $(\Delta F_c)_{i+1}$ to $(\Delta y_c)_{i+1}$ gives the numerical approximation of the stiffness at the point of fixel-workpiece contact corresponding to the current configuration (L_1 and $\theta_{2_{i+1}}$).

This procedure is then repeated by keeping the length of the base link fixed and varying the base angles through the kinematic range of values to obtain different stiffness values for the different configurations (L_1 and θ_2's). Another set of stiffness values is then obtained by

changing the base length to another value (say L_2) from the known range and repeating the procedure for all possible base angles. These stiffness values correspond to the new set of configurations (L_2 and θ_2's). By repeating this procedure for all base lengths and all base angles within the allowable range, a final set of all the possible stiffness values (along y-direction) is obtained. Thus, using this fixel design, adjustable fixel stiffness can be achieved by varying the two mechanical parameters – the base length and the base angle of the fixel.

3.1.5 Derivation of Stiffness of the Fixel Along x-direction

The stiffness of the fixel along the x-direction for all possible values for L_1 and θ_2 in the kinematic range of values are calculated by following the procedure similar to the derivation of the stiffness along y-direction. The value of the contact force along the x-direction ($F_{C_{xi}}$) is calculated using Equation 3-3. The value of x-coordinate of the point of contact (x_{C_i}) is calculated using the expression for x_c shown in Equation 3-2. Repeating all the steps followed in section 3.1.4, a final set of all the possible stiffness values (x-direction) for all base lengths and all base angles within the allowable range is obtained.

Hence, the Design 1 provides directional adjustable stiffness characteristics in X and Y, and has two mechanical variables for adjustment.

3.2 Design 2

Fixel Design 2 is a cantilever beam fixel with unidirectional variable stiffness characteristics. This design is a basic cantilever beam (beam fixed at one end) with contact between the workpiece and the fixel occurring at its free end. For a cantilever beam, the minimum value of *k*, or stiffness, occurs at the free end of the beam. For a given material, this minimum *k* is a function of the length *L* of the beam measured from the fixed end and its moment of inertia *I*. For the designs shown herein, the fixels are assumed to have rectangular

cross-sectional areas with breadth *b* and width *h*. Thus, it is understood that *k* is a function of *L* and *h* and this dependency is advantageous in designing fixels. For the cantilever beam type fixel designs proposed in this section, the mechanical adaptability is achieved individually varying *L* or *h*. Thus, for these designs, there is a single mechanical parameter (single actuation) unlike Design 1.

3.2.1 Design 2a) – Mechanical Variable L

The cantilever beam type fixel for Design 2a is shown in Figure 3-5. The integration of the four fixels with the workpiece setup is shown in Figure 3-6 which consists of the cantilever/compliant beam, the fixture base module and the interface element. To decouple residual motions from occurring when making changes in the mechanical variables, the fixel contact with the workpiece is acquired via the interface component. One end of the interface component has direct contact with the workpiece and the other end is connected to a point on the cantilever beam (near the free end). The contact force F_C between the workpiece and the fixel acts along the interface element and occurs at this point on the cantilever beam. This contact force will vary depending on the loads involved in the machining process. The fixture module clamps the cantilever beam at the base, with the length of the beam *L* being defined as the distance between this fixed/constrained end and the point of action of the contact force (near the free end of the beam).

Using the cantilever beam equation for stiffness, the principle involved in fixel Design 2a is to adjust the stiffness *k* at the point of fixel-workpiece contact (near the free end of the cantilever beam) by modifying the beam length *L*. Mathematically, the stiffness can be expressed as shown in Equation 3-6 where for fixel Design 2a, $\alpha = 3EI = Ebh^3/4$ and is a constant, and the mechanical variable is *L*.

$$k = \frac{3EI}{L^3} = \frac{Ebh^3}{4L^3} = \frac{\alpha}{L^3} \tag{3-6}$$

In response to the fixturing needs, the length of the cantilever beam could be controlled by unclamping the beam from the fixture module base and then moving it by the required length; thus changing the effective beam length L (as illustrated in Figure 3-6). In this design approach, the value of k given by Equation 3-6 can be adjusted passively during fixturing set up as well as actively during the process.

For the Design 2a's fixel, the minimum value of k would occur when the length is L_{max} and maximum value of k corresponds to L_{min} as shown in Equations 3-7 and 3-8.

$$k_{\min} = \frac{Ebh^3}{4L_{\max}{}^3} = \frac{\alpha}{L_{\max}{}^3} \tag{3-7}$$

$$k_{\max} = \frac{Ebh^3}{4L_{\min}{}^3} = \frac{\alpha}{L_{\min}{}^3} \tag{3-8}$$

For the purpose of comparisons between fixel designs, a new parameter r is introduced which is defined as the ratio of minimum to maximum values of the fixel's mechanical variables. This ratio provides a dimensionless measure for quantifying the mechanical variable's range of motion, facilitating the comparison of the different fixel design types. For Design 2a, r is the ratio of L_{min} to L_{max} and substituting r into Equation 3-7 results in the Equation 3-9 which provides a relationship between the design constants (material and geometric parameters), k_{min}, and the range of motion of the mechanical variables r.

$$k_{\min} = \frac{Ebh^3 r^3}{4L_{\min}{}^3} = \frac{\alpha r^3}{L_{\min}{}^3} \tag{3-9}$$

Hence, for Design 2a, L_{min} and r are the two unique parameters. The selection of L_{min} and r determine the value of L_{max} and by varying L from L_{min} to this calculated L_{max}, a set of values of k

that are achievable for each given fixel design are obtained. For investigating the mechanical adaptability of the fixel, the design variations of Design 2a are explored for different sets of the design parameter r for a given L_{min} and k_{min}.

3.2.2 Design 2b) – Mechanical Variable h

The cantilever beam type fixel for Design 2b is shown in Figure 3-5. The integration of the fixel with the workpiece setup is shown in Figure 3-7 which is similar to Design 2a (four fixels). In this design, the length of the cantilever is held constant and the adjustable fixel stiffness is achieved by varying the width h of the beam as shown in Figure 3-7. This can physically be achieved by adding multiple strips of same length and breadth to the cantilever beam thus changing the effective width h'. The effective width can be calculated using the Equation 3-10 where n is the number of thin strips and Δh is the width of each thin strip.

$$h' = h + n(\Delta h) \tag{3-10}$$

Since Δh has to be increased discretely (unlike L in Design 2a), a very small value of Δh can be chosen such that the change in k is equal to the least count of the system (the least value of change in k required).

The value of h' (and thereby the number of thin strips) needed to obtain a required k can be calculated using Equation 3-10. The width could be changed from a minimum value of h_{min} to a maximum value of h_{max} which would correspond to a minimum and maximum value for fixel stiffness k given by the Equations 3-11 and 3-12 where for fixel Design 2b β would be a constant defined as $\beta = Eb/4L^3$ and the mechanical variable is h.

$$k_{\min} = \frac{Eb{h_{\min}}^3}{4L^3} = \beta {h_{\min}}^3 \tag{3-11}$$

$$k_{\max} = \frac{Eb{h_{\max}}^3}{4L^3} = \beta {h_{\max}}^3 \tag{3-12}$$

Similar to Design 2a, introducing r as the ratio of h_{min} to h_{max} and substituting r into Equation 3-11, results in Equation 3-13.

$$k_{\min} = \frac{Ebr^3 {h_{\max}}^3}{4L^3} = \beta r^3 {h_{\max}}^3 \tag{3-13}$$

Here, h_{max} and r are the two unique parameters of Design 2b and fixed values for these parameters determine the value of h_{min}. By varying h from h_{max} to this newly calculated h_{min}, one obtains the set of values for k that are achievable for each given design. Similar to the previous design, the variations of Design 2b are explored for different sets of the design parameter r for a given h_{max} and k_{min}. These results will be compared with the designs of other fixels to further delineate their effectiveness.

3.3 Design 3

The fixel for this design consists of a beam fixed at both ends as shown in Figure 3-8. The workpiece would be held via contact with one end of an interface element (similar to Design 2a) where the interface element connects at some point along the beam. Figure 3-9 is an illustration for the implementation of Design 3 using four fixels to hold the workpiece. Each contact point would be at a distance x from a fixed end and the contact force F_C acting along the interface element will be exerted on the beam at this point. By moving the beam along the direction of its axis and by allowing the end of the interface element to roll on the beam, the contact force point of application can be changed without inducing any motion of the workpiece. The new value of x obtained by this change would correspond to the value of k required at this instance. This value of x can be calculated using the relationship between k and x given by Equation 3-14 where L is a fixed length and γ is a constant defined as $\gamma = 3EI = Ebh^3/4$.

$$k = \frac{\gamma L^3}{x^3 \left(L - x\right)^3} \tag{3-14}$$

Thus, in this design, the stiffness k can be controlled by varying the point of application of the contact force (F_C), i.e., by adjusting the mechanical variable x. The distance of the contact point can be varied from a minimum value of x_{min} to a maximum value of x_{max} where x_{max} will be half the fixed length L of the beam (due to the symmetry of the fixel system). The corresponding minimum and maximum values of k are given by the Equations 3-15 and 3-16.

$$k_{\min} = \frac{2Ebh^3}{{x_{\max}}^3} \tag{3-15}$$

$$k_{\max} = \frac{Ebh^3L^3}{4{x_{\min}}^3\left(L - x_{\min}\right)^3} = \frac{\gamma L^3}{{x_{\min}}^3\left(L - x_{\min}\right)^3} \tag{3-16}$$

Introducing r as the ratio of x_{min} to x_{max} and substituting r into Equation 3-16 results in the Equation 3-17 below.

$$k_{\max} = \frac{2Ebh^3}{r^3\left(2 - r\right)^3 {x_{\max}}^3} \tag{3-17}$$

Here, x_{max} and r are the two unique parameters of Design 3. Also, similar to the previous designs, fixed x_{max} and r values will determine a unique value of x_{min}. Again, similar to the previous designs, for a fixed x_{max} and for different sets of the design parameter r, different variations of Design 3 are obtained. Each design variation results in a set of k values that can be achieved from varying its mechanical variable (x) from x_{min} to x_{max}.

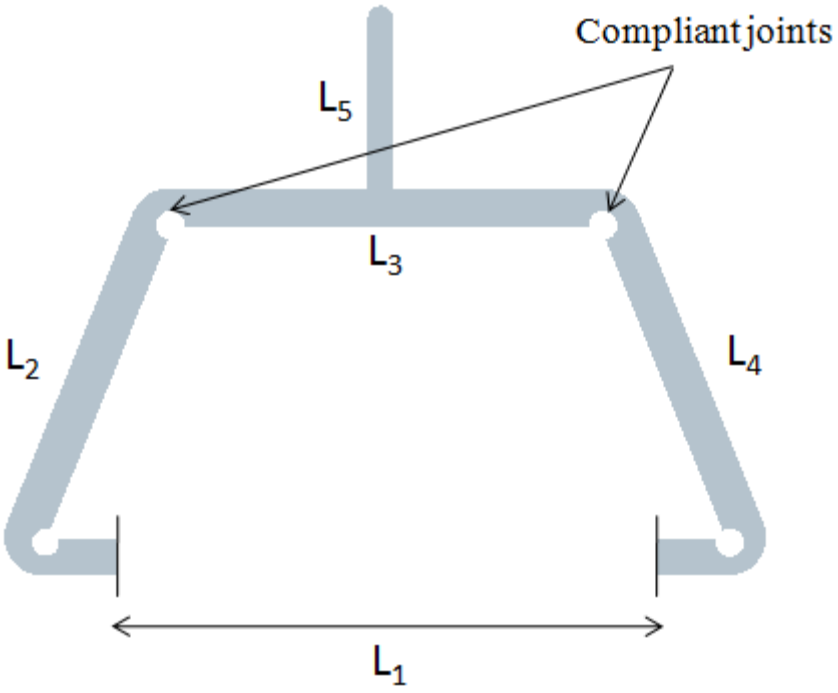

Figure 3-1. Design 1 – Simple monolithic compliant four-bar mechanism consisting of four compliant joints

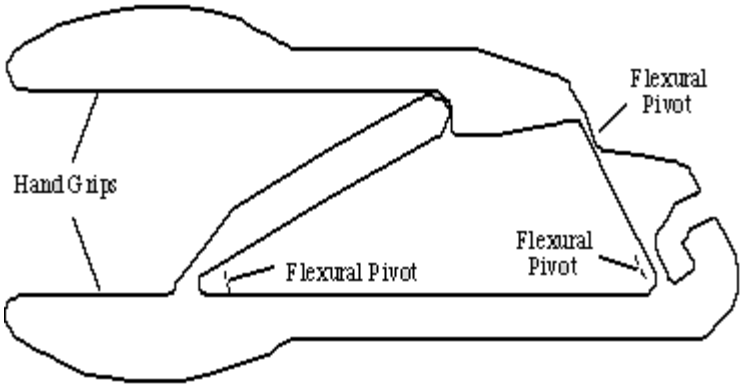

Figure 3-2. Example of a Compliant Mechanism – a Crimping Mechanism consisting of three flexible members (courtesy of Compliant Mechanisms by Larry Howell)

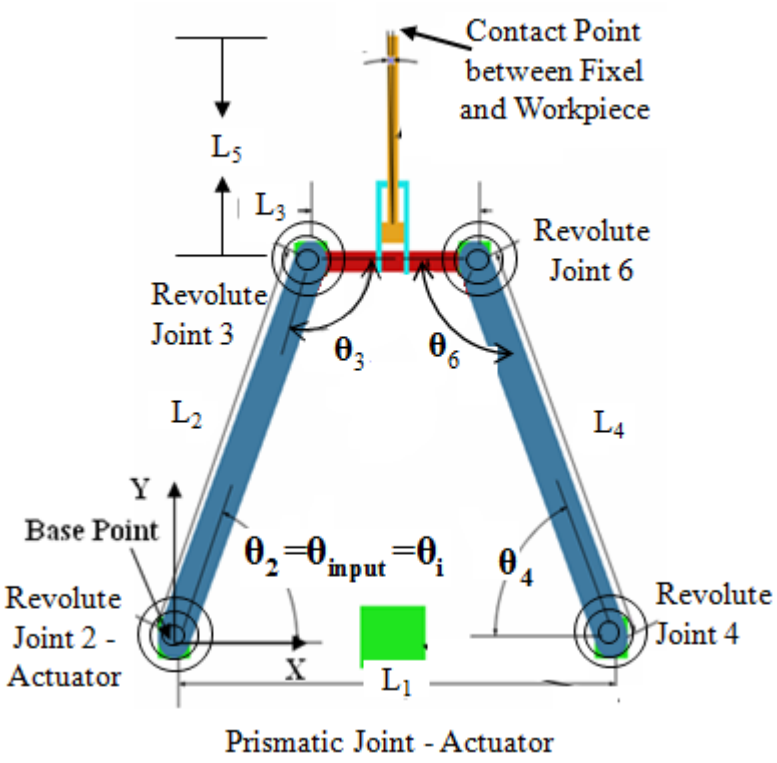

Figure 3-3. Pseudo Rigid Body Model for the Four bar monolithic fixture

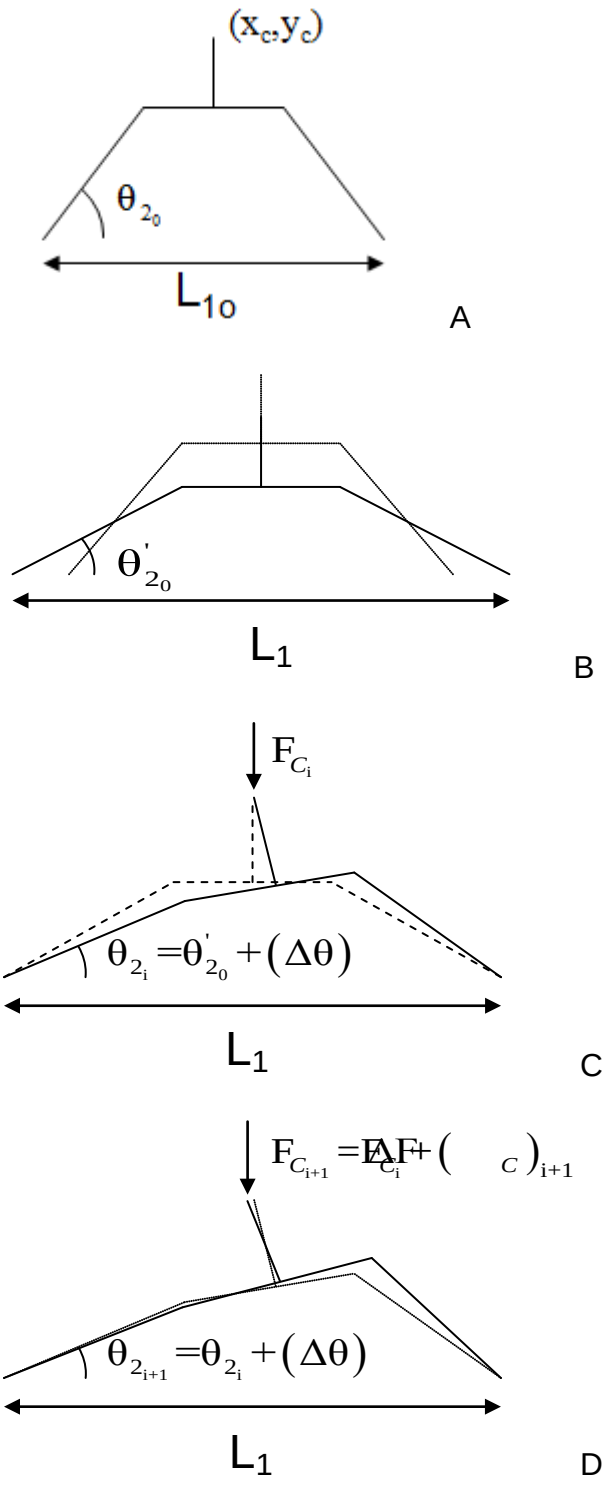

Figure 3-4. The various configurations of Design 1 during stiffness calculations - a) Initial Configuration b) Symmetric Equilibrium with Base Length L_1 c) Displacement Due to Contact Force with Base Length L_1 d) Change in Displacement Due to a Change in Contact Force with Base Length L_1

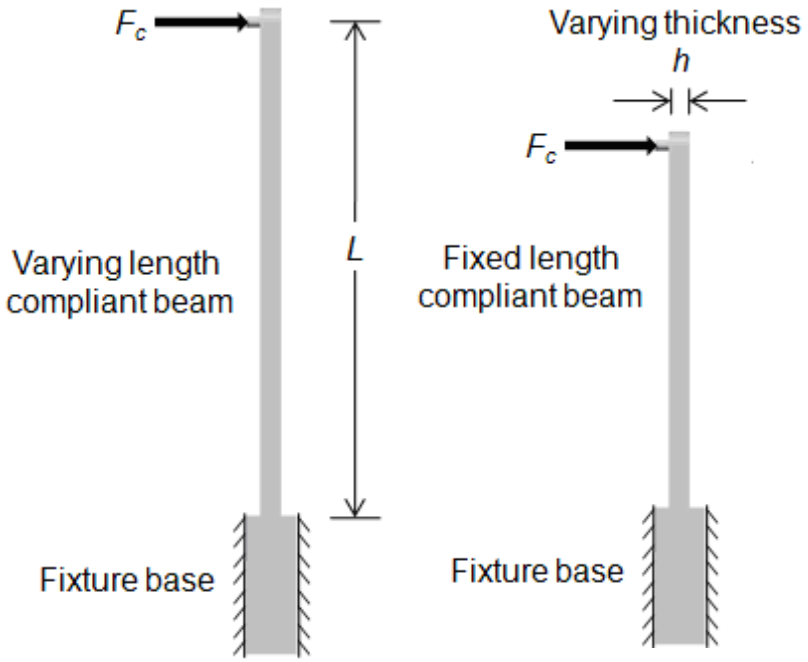

Design 2a) **Design 2b)**

Figure 3-5. Design 2 – Principles Involved

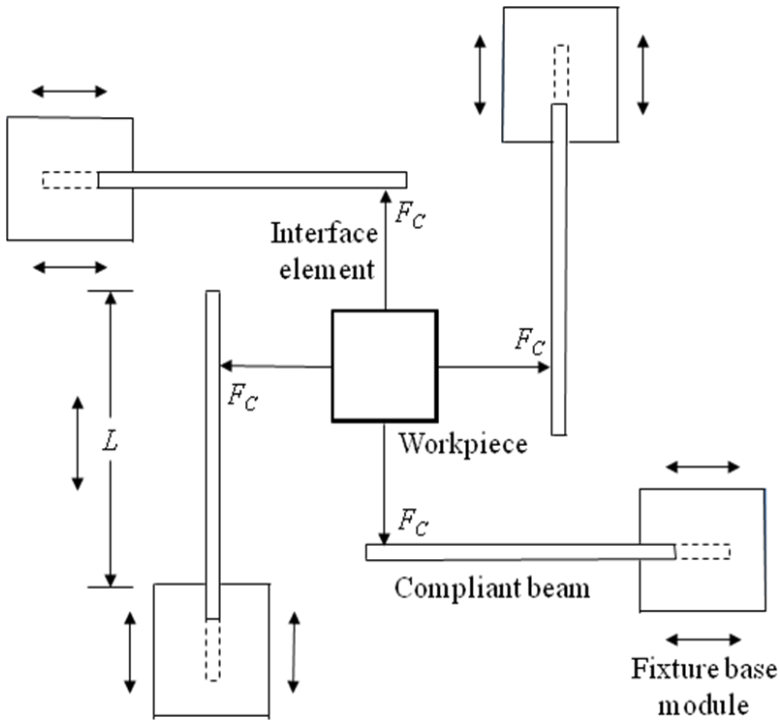

Figure 3-6. Implementation of Design 2a with Four Fixels

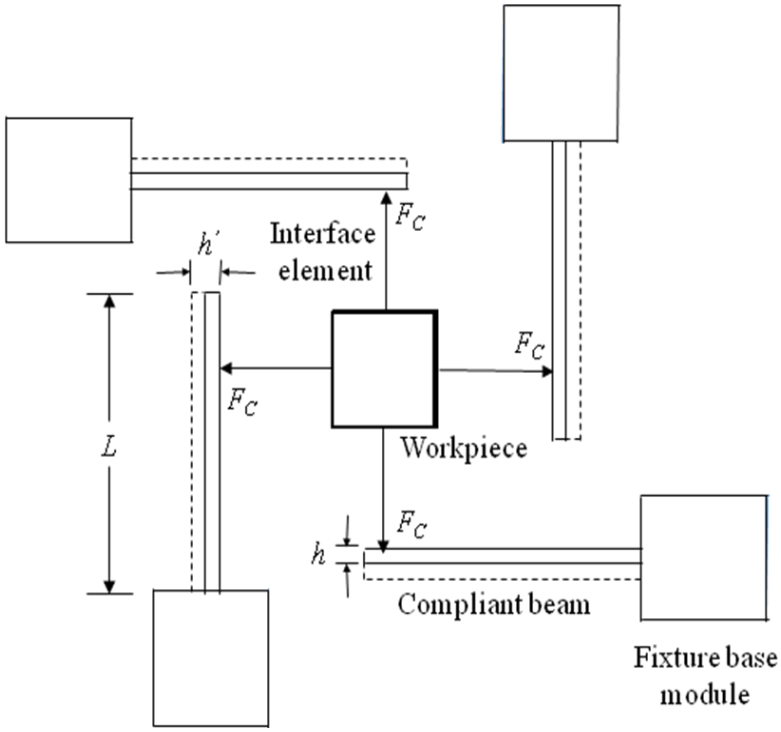

Figure 3-7. Implementation of Design 2b with Four Fixels

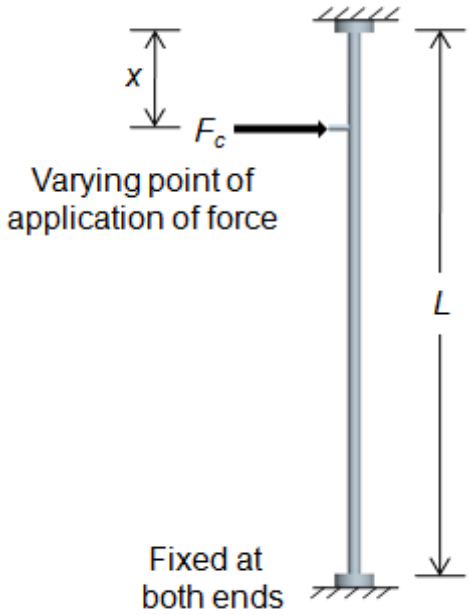

Figure 3-8. Design 3 – Principle Involved

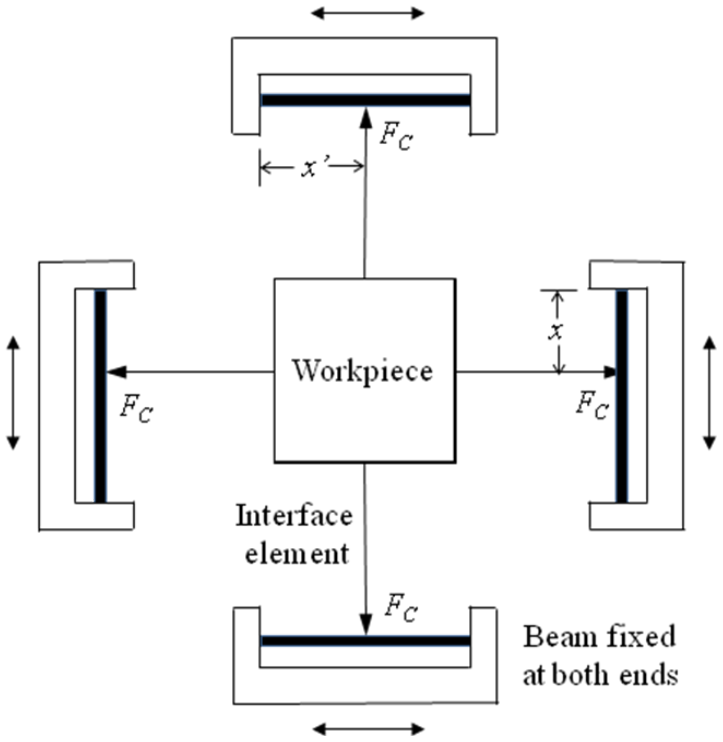

Figure 3-9. Implementation of Design 3 with Four Fixels

CHAPTER 4
COMPARISON OF THE DESIGNS

After establishing the principles of the designs and the relationships between fixel stiffness and the mechanical parameters of the designs, the fixel stiffness at the fixel-workpiece contact are plotted for Design 1. This is followed by a comparison of the stiffness characteristics of the similar compliant beam designs 2a, 2b and 3.

4.1 Design 1

For the Design 1 proposed in section 3.1, results were generated for the fixel design with constant parameters L_2=L_4=45mm, L_3=30mm and all torsional springs having equal spring constants. The link lengths were chosen to exhibit the same relative footprint as Designs 2 and 3. The fixel stiffness as seen at the point of fixel-workpiece contact for the four-bar type fixel is plotted as a function of the two mechanical variables (L_1, θ_2) by following the procedure mentioned in the section 3-1. The kinematic range of values for L_1 is chosen from 45mm to 55 mm and the range of values for θ_2 for these link lengths was obtained to be from 40 degrees to 60 degrees. This plot for fixel stiffness with respect to L_1 and θ_2 is shown in Figure 4-1.

In the Figure 4-1, a dynamic symmetry is observed for the mechanical variable θ_2 for each value of L_1. This symmetry can be attributed to the design constraints of L_2=L_4, joint flexures of equal stiffness and to the method of calculating the range of θ_2 from one toggle position to another. Because of the dynamic symmetry, it is observed that the trend in the fixel's stiffness is independent of the length of the base link. This is apparent in the Figure 4-1 by observing the different contours in θ_2 for different L_1. However, the magnitudes of the base link length impact the actual instantaneous stiffness values and thus the dynamic range of stiffness achievable for a given range of the base angles. For example, an L_1=45mm fixel configuration exhibits higher range of stiffness values achievable as compared to L_1=55mm fixel configurations.

It is also observed that for the L_1=45mm fixel configuration, a local minimum about its unloaded equilibrium configuration ($\theta_2 \approx 50$ deg) exists and therefore deviations from this configuration will take less effort. While for L_1=55mm fixel configuration at its unloaded equilibrium configuration, the fixel exhibits a peak stiffness value and will be resistant to changes from this configuration. It is also observed that the range of stiffness values achievable is lesser for smaller base length values. Due to the presence of these variations in the trends, it is observed that Design 1 will provide for greater control diversity in tuning the fixture dynamics via actuating the base length (L_1) and input angle (θ_2) either individually or together.

4.2 Comparison of Designs 2a, 2b and 3

Arbitrarily considering values for each fixel's fixed and unique design parameters, would not yield a discernable comparison of the different types of fixel designs. Thus, to compare Designs 2a, 2b and 3, a common range of values of k achievable for all three designs is determined. It is known from the previous section that each of the three beam type designs have a particular k_{min} value for given r and fixed design parameters. Hence, for more equitable comparison between the Designs 2a, 2b and 3, this minimum value of k for each of the designs with same specified value of r were made equal. Equations 4-1 to 4-3, shown below, are obtained by equating k_{min} and r values of each of the designs.

$$k_{\min} = \left.\frac{Ebh^3r^3}{4{L_{\min}}^3}\right|_{\text{design 2a}} = \left.\frac{Ebr^3{h_{\max}}^3}{4L^3}\right|_{\text{design 2b}} = \left.\frac{2Ebh^3}{{x_{\max}}^3}\right|_{\text{design 3}} \tag{4-1}$$

$$\frac{k_{\min}}{Eb} = \frac{h^3r^3}{4{L_{\min}}^3} = \frac{r^3{h_{\max}}^3}{4L^3} = \frac{2h^3}{{x_{\max}}^3} \tag{4-2}$$

$$r = \frac{L_{\min}}{L_{\max}} = \frac{h_{\min}}{h_{\max}} = \frac{x_{\min}}{x_{\max}} \tag{4-3}$$

By restricting that all designs have the same minimal fixel stiffness (k_{min}), the value of k_{max} at r equals 1 is also found to be the same for all three designs. Note, when r equals 1, the range of motion of the mechanical variable is restricted to be zero, thus resulting in the loss of the variable stiffness feature of the fixel. With this common window of constraints on the stiffness values formed by the k_{min} restriction, the values of k_{max}, Δk (equal to $k_{max} - k_{min}$) and the average slope of k (Δk by change in the varying parameter of the design) for the intermediate values of r, the different beam type fixel designs can be compared more directly.

For Equation 4-1 to yield a viable comparison, it was assumed that the breadths (b) of the beams of each design are equal and that the material of the beam is also the same. Furthermore, the constant beam width h of Design 2a was made to be equal to h_{min} of Design 2b, and the constant beam width h of Design 3 was made equal to r times h_{min} of Design 2b. Similarly, the constant length L of Design 2b was made equal to L_{min} of Design 2a and x_{max} of Design 3 was made to be twice L_{min}. This leads to the different beam type fixel designs having the same lower bound on the slenderness ratio.

The slenderness ratio (s) of a beam is defined as the ratio of the minimum length of the beam to its maximum width. For the different beam type fixel designs, the following relationships shown in Equations 4-4 and 4-5 yield the lower bound on s.

$$s = \frac{L_{\min}}{h_{\max}} \qquad \text{for Designs 2a and 2b} \tag{4-4}$$

$$s = \frac{2x_{\max}}{h_{\max}} \qquad \text{for Design 3} \tag{4-5}$$

where, from the assumptions of Euler-Bernoulli beam theory, s should be greater than 10.

To determine L_{min}, the size of the workpiece has to be considered. Assuming that the workpiece has a size of 10mmx10mmx10mm, a safe estimate for L_{min} is given by Equation 4-6.

$$L_{\min} = 10\ mm \tag{4-6}$$

From specified values of L_{min}, r and s, the parameters of comparative fixel designs and the corresponding k values can be obtained by the following procedure:

4.2.1 Design 2a

Equation 4-6 gives the value of L_{min}

Using the specified value of s, the value of h_{max} can be obtained from Equation 4-4. Then using Equation 4-3 and the specified value for r, h_{min} can be calculated to determine the constant beam width h as shown by Equation 4-7.

$$h = h_{\min} \tag{4-7}$$

Using Equation 4-3 with the same value of r, the value of L_{max} can be obtained from the known value of L_{min}.

For each fixel design variation defined by specified values of s and r, a range of values for L varying from L_{min} to L_{max} is obtained which correspond to a range of values of k.

4.2.2 Design 2b

Equation 4-6 gives the value of L_{min} which would be equal to the constant beam length L of this design as shown by Equation 4-8.

$$L = L_{\min} \tag{4-8}$$

Values of h_{max} and h_{min} for specified values of s and r are the same as that obtained above in Design 2a.

A range of values for h varying from h_{max} to h_{min} is thus obtained which correspond to a range of values of k.

4.2.3 Design 3

As previously explained, x_{max} is twice the value of the L_{min} obtained from Equation 4-6 which can be expressed as Equation 4-9.

$$x_{\max} = 2L_{\min} \tag{4-9}$$

Also, the constant width of the beam would be r times h_{min}. Using the known value of h_{min} from Design 2a calculations, the fixed width can be calculated using Equation 4-10 shown below.

$$h = rh_{\min} \tag{4-10}$$

The value of x_{min} for specified values of r can then be determined by substituting the value of x_{max} into Equation 4-3.

For specified values of s and r, a range of values of x varying from x_{max} to x_{min} is obtained which correspond to a range of values of k.

4.2.4 Plots for Design 2a, 2b and 3

For each of the above beam type fixel designs, k_{min}, k_{max}, Δk and average slope of k were plotted as a function of r and s (r varies from 0.1 to 1 and s varies from 10 to 30). Figures 4-2 through 4-9 are the normalized plots of the stiffness quantities (k_{min}, k_{max}, Δk and average slope of k) with respect to (Eb). These results provide the trends for each design independent of the fixel's material properties. Figure 4-2 demonstrates that all the three designs have the same instantaneous k_{min} values, shown as a function of r and s. Figures 4-3 and 4-4 demonstrate the variation of k_{max} for various combinations of [r, s]. It is found that all the designs have the same maximum possible k_{max} value (which occurs at r=1 and s=10). However, the variation of k_{max} as a function of r and s is different for Design 3. Figures 4-5 and 4-6 represent the variation of Δk (difference between k_{max} and k_{min}) for the three beam type designs. Figures 4-7 through 4-9 are

the plots for the average slopes of k, where the average slopes are calculated as the ratio of Δk over the range of the change in the mechanical variable corresponding to each of the designs.

From these plots, it is observed that the range of k's achievable reaches a maximum at around $r \cong 0.8$ for all slenderness ratios. Also, a smaller s (shorter or thicker beams) yields a greater range in k. For Design 2b, a smaller value for s results in a larger h_{max} value for given L_{min} which has the effect of increasing the range of the mechanical variable h and thus increasing the range of k. This increase in h_{max} effects the h of Design 2a which in turn has a similar amplification affect on this design's resulting range of k. The Δk are also found to be higher for Designs 2a and 2b than that of Design 3 (by a factor of 7). For an overall measure of k variations between k_{min} and k_{max}, Design 2b trends were found to be a factor of 10 higher in average change in k, as compared to Designs 2a and 3. This indicates that Design 2b has greater mechanical adaptability for a given range in variable (defined by r).

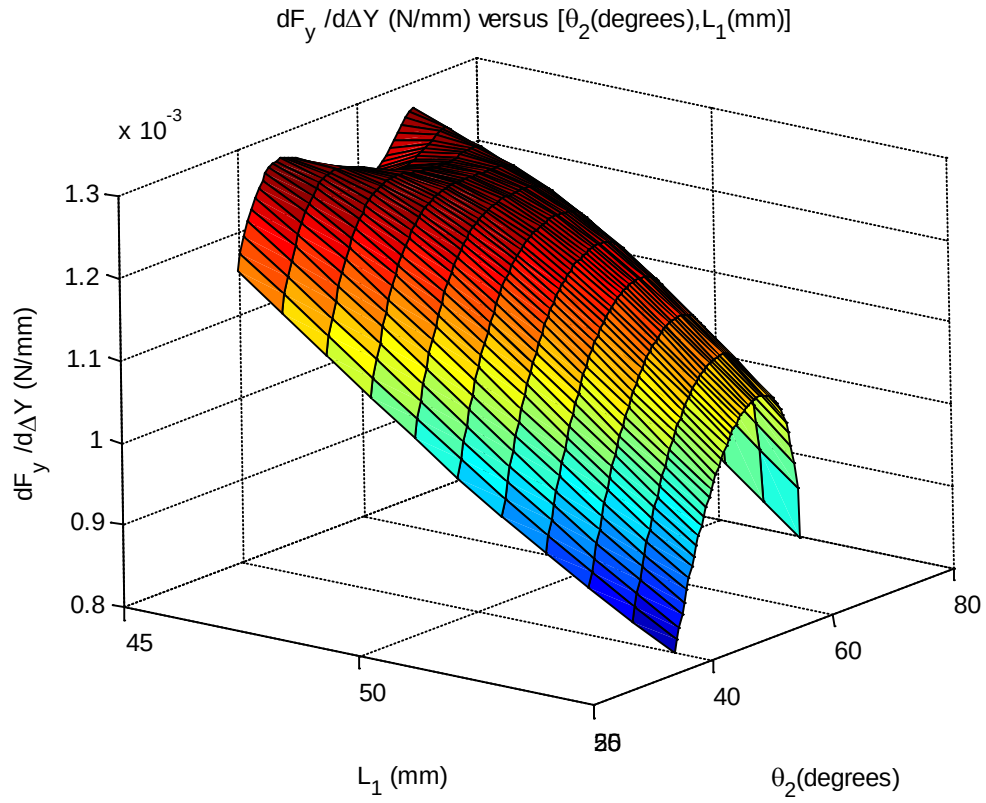

Figure 4-1. Fixel Stiffness (L_2=L_4=45mm, L_3=30mm, all k's are equal)

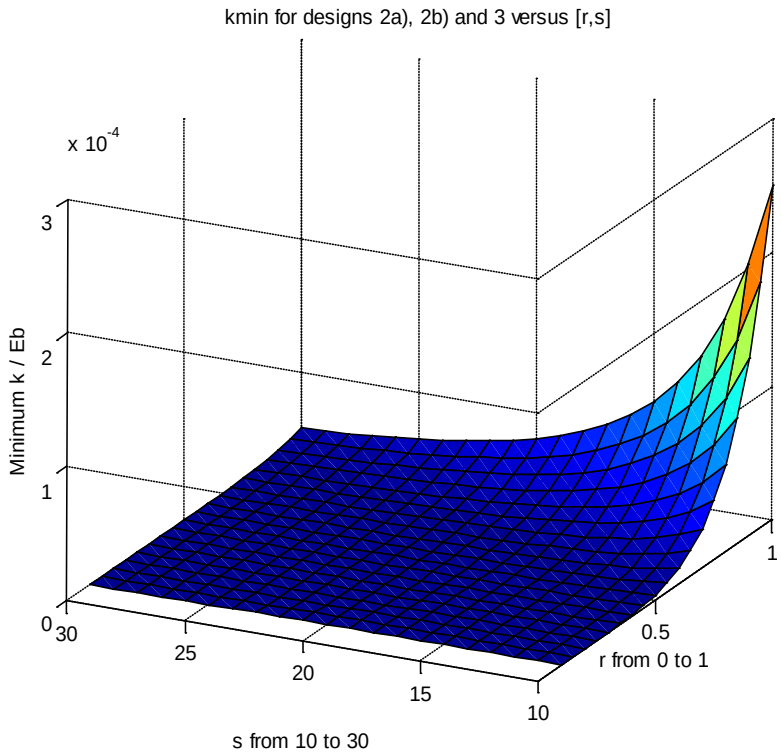

Figure 4-2. (k_{min} /*Eb*) for Designs 2a, 2b and 3 versus [*r*,*s*]

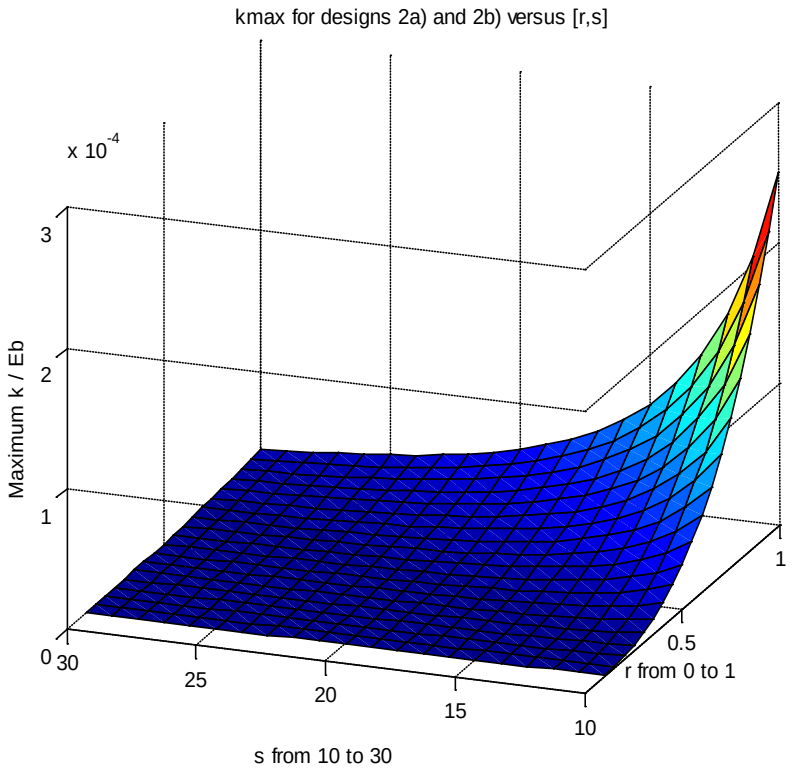

Figure 4-3. (k_{max} /*Eb*) for Designs 2a and 2b versus [*r*,*s*]

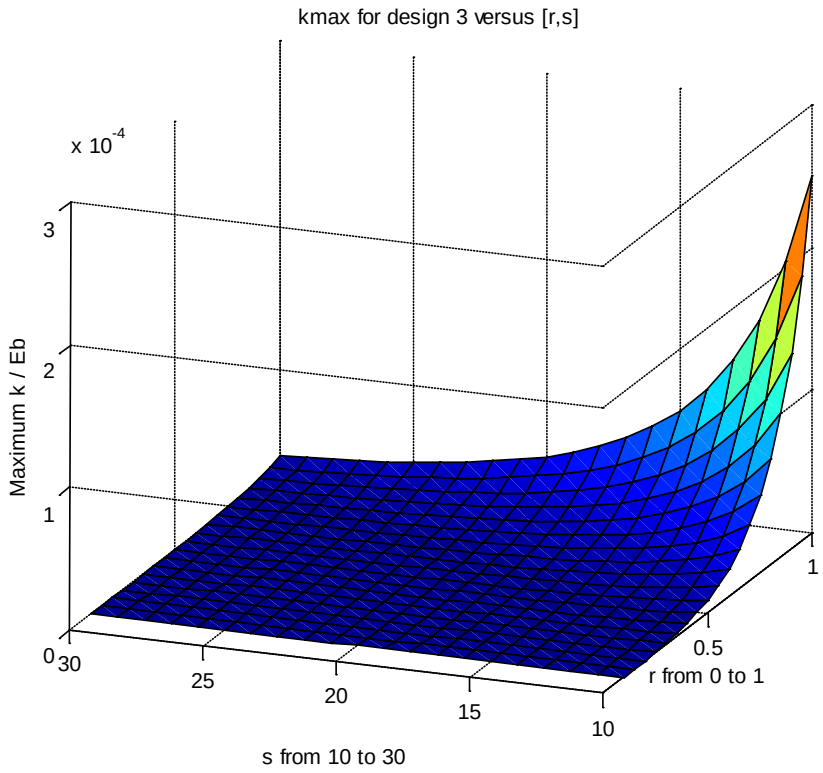

Figure 4-4. (k_{max} /*Eb*) for Design 3 versus [*r*,*s*]

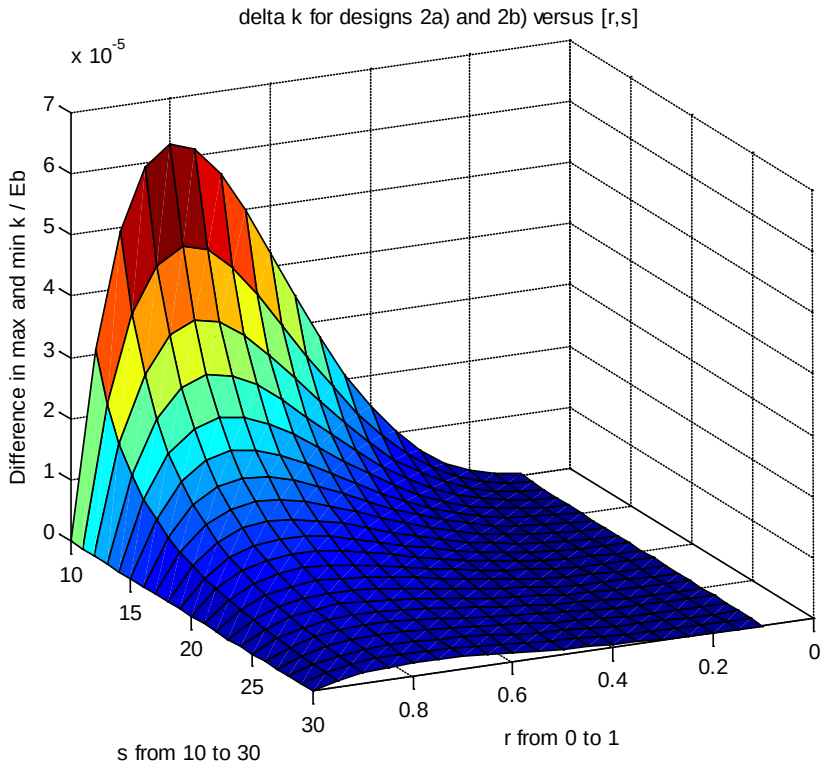

Figure 4-5. (Δk /Eb) x 10^{-5} for Designs 2a and 2b versus [r,s]

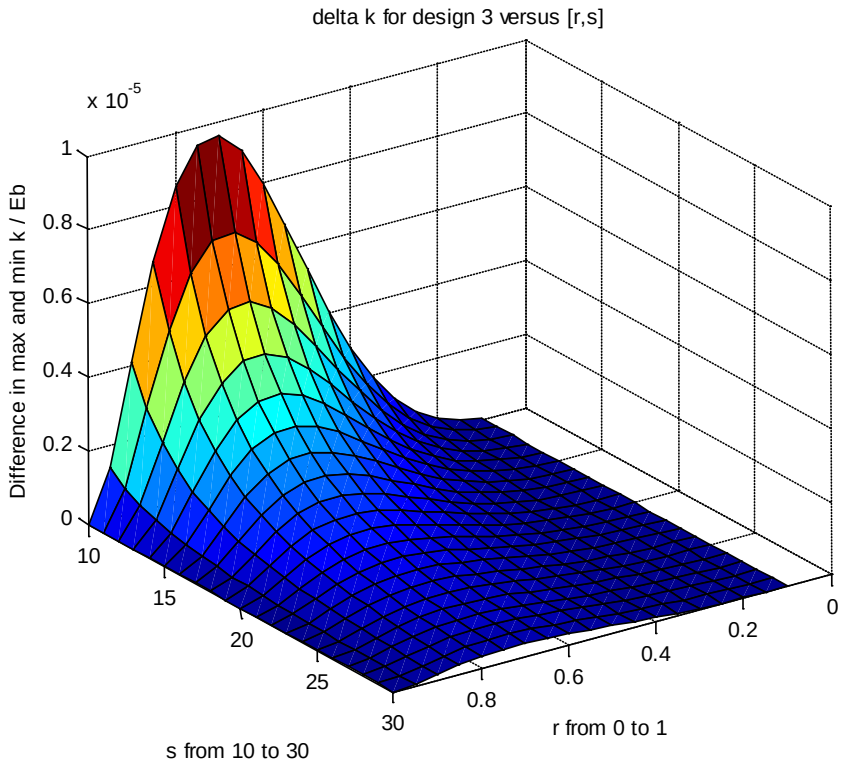

Figure 4-6. ($\Delta k / Eb$) x 10^{-5} for Design 3 versus [r,s]

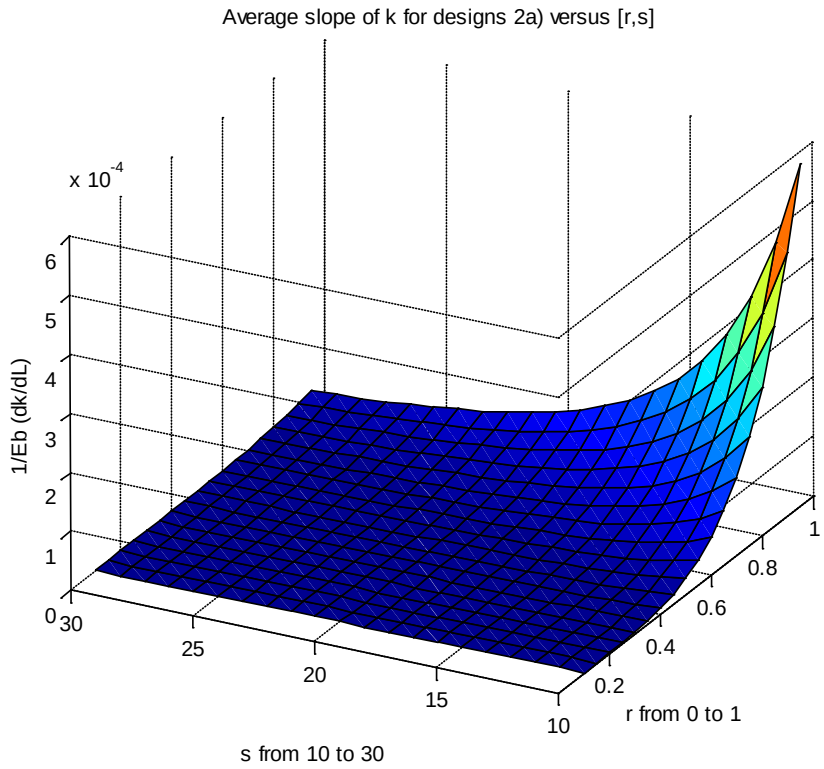

Figure 4-7. (Average Slope of k /Eb) x 10^{-4} for Design 2a versus [r,s]

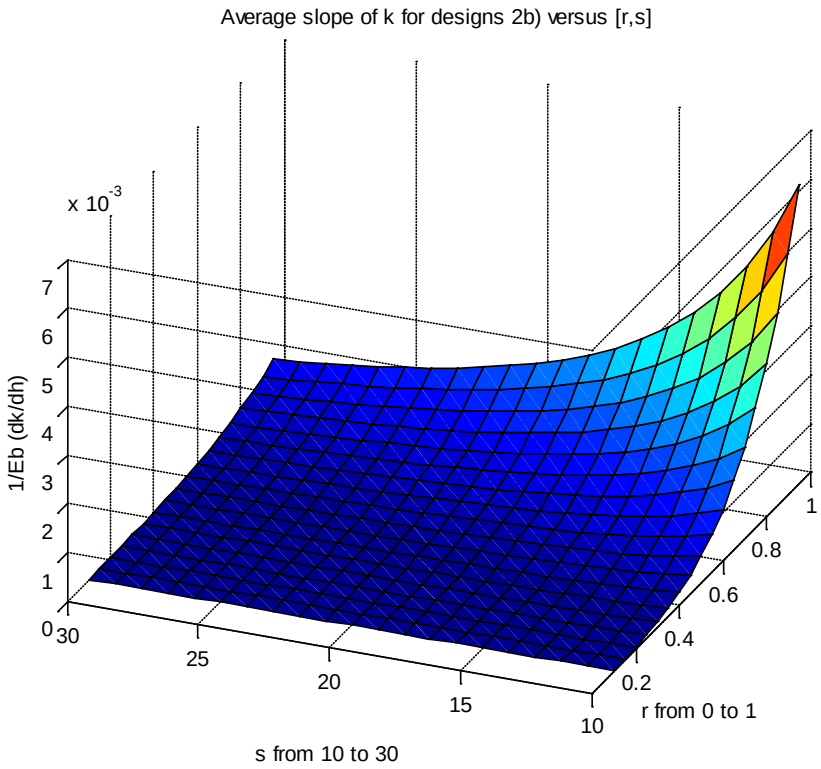

Figure 4-8. (Average Slope of k /Eb) x 10^{-3} for Design 2b versus [r,s]

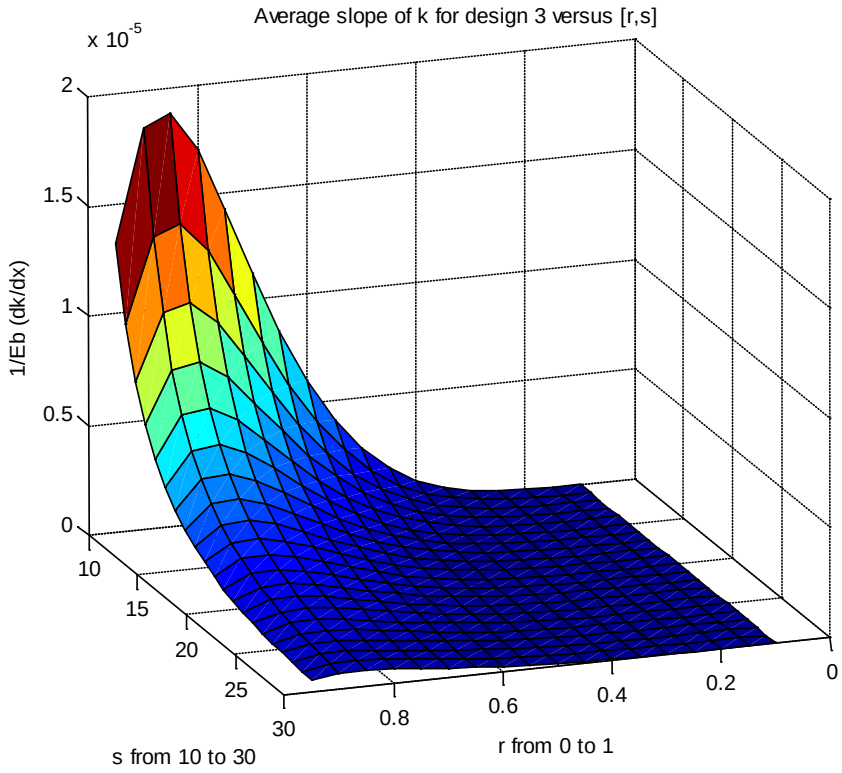

Figure 4-9. (Average Slope of k /Eb) x 10^{-5} for Design 3 versus [r,s]

CHAPTER 5
ANALYSIS OF THE FIXEL DESIGNS

In this chapter, a fixel design is incorporated into a machine tool setup and the performance of the design under operation conditions subject to runout induced errors is analyzed. The fixel design and the number of compliant fixels (of that design) used in a setup will depend on the type of manufacturing process. For example, in case of a meso scale drilling process at least four fixels of Design 1 are required. The (X, Y) directional stiffness characteristics of fixels of Design 1 integrated in a coordinated manner is best suited for achieving the preferred fixturing capabilities and accurate drilling. In the case of a milling process, two fixels of any of the four designs are theoretically required to achieve fixturing capabilities. Because each of the designs have the same principle of utilizing adjustable stiffness characteristics, the following analysis is done without loss of generality for only one of the designs for a particular meso manufacturing process. The results of this analysis can be extended to other designs and processes. For the purpose of this study, Design 2a is selected for analysis and is implemented in an end milling machine tool system which has runout in the direction perpendicular to feed. Another example of such a system could be a burnishing setup where a mesoscale workpiece with micro features is being burnished for improved finishing. When the tool is burnishing the surface of the workpiece which is close to the feature, the runout in the tool (perpendicular to the feed) inadvertently affects the dimensions of feature during the burnishing process.

One more mesoscale manufacturing setup which can have runout in the perpendicular direction to the feed is a peripheral milling setup with runout error occurring due to variation in teeth lengths. Considering that in such a setup, one of the teeth of the cutter is longer than the other teeth, the excess length of the longer teeth corresponds to the runout error. Such runout errors in a peripheral milling setup results in varying depth of cut and this error can be

compensated by following the same procedure as that for the end milling setup which is explained in Section 5.1 below.

5.1 Static Analysis of Design 2a

The fixture workpiece setup for an end milling operation with two fixels of Design 2a) and two rigid fixels is shown in Figure 5-1. The fixture-workpiece is fixed to the platform of the milling machine such that the rigid fixels are aligned parallel to the direction of motion of the platform. These rigid links counter the cutting force during the milling operation. Assuming for the current setup, that the tool on the milling machine has radial runout in the direction perpendicular to the cutting direction, the compliant fixels are aligned in this direction. Due to this runout, the thickness of the slot being machined into the workpiece is larger than the required value. The perpendicular runout of the tool in such a system results in a force (extraneous to cutting force) acting on the workpiece which then acts along the interface element of the compliant fixel. Since the interface element is connected to the variable length compliant beam at its free end, it leads to the bending of the beam which then results in a corresponding displacement of the workpiece. The rigid fixels slide freely in this direction without their contact with the workpiece slipping so that it does not introduce any resistance to the compliant fixture's corrective displacement of the workpiece. The objective of the current approach is to improve the accuracy of dimensioning in spite of errors resulting from runout by constantly controlling the beam deflection such that it is always equal to the runout value. This eventually results in no relative motion between the tool and the workpiece from its theoretical nominal cutting trajectory, thus mitigating the adverse affects on the dimensional accuracy of the finished workpiece. The value of beam deflection x will be a function of the contact force F_c (created because of the tool runout) and the stiffness of the beam k which in turn depends on the length of the beam L as shown in Equation 5-1.

$$F_c = \frac{Ebh^3}{4L^3} x \tag{5-1}$$

If the runout value (and the corresponding non-proportional contact force) changes during the process, the length of the beam can be adjusted so that the deflection of the beam is now equivalent to this new runout value thus maintaining the desired thickness of the slot. The runout values can be dynamically measured using Non-contact Precision Capacitance Sensors.

To prove this concept of achieving beam deflection equivalent to the runout, a ProE model of a single fixel and the workpiece along with appropriate constraints is modeled as shown in Figure 5-2. The mesoscale size of the workpiece is chosen as 5 mm x 5 mm x 5 mm. A set of values of the required runouts are initially chosen (similar to values found in literature [12]). To calculate the range of values of the contact forces, a value of 8 mm is chosen for *L* and the expected runout is chosen (from known range of values) as 0.06 mm. Using Equation 5-1, the value of contact force is calculated to be in the order of 25 mN. Now, the value of the contact force is varied in the range of 20 mN to 30 mN and the values of *L* corresponding to a range of runouts are calculated using Equation 5-1. The contact force is not necessarily proportional to the runout and keeping this in mind, different combinations of contact force and runout values are chosen to calculate the *L* values. To validate these estimated lengths using the model, the length of the compliant beam in the model is set to one of the calculated values of *L* and the corresponding contact force is applied to the workpiece. A force analysis is done on this model and the deflection of the beam is obtained as shown in Figure 5-3. The value of the beam deflection is then compared to the value obtained from the formula. Since, the formula is obtained after making certain assumptions, these values vary by a small amount. Similar values of *L* were obtained for different sets of runout and contact forces and are tabulated in Table 5-1 which shows the possibility of achieving different runout compensation by varying the length of

the compliant beam. This is again shown in the form of a graph in Figure 5-4. These values of length and corresponding stiffness values may or may not be the same for the analysis under the influence of a harmonic force.

5.2 Analysis of Design 2a Under Harmonic Force

The next step is to analyze the design under the operation conditions of a mesoscale milling setup. Assuming that there exists runout in the tool of such a system, it results in a harmonic force *F* (as shown in Equation 5-2) acting on the workpiece which in turn acts on the compliant beam. The frequency of this harmonic force will be equal to the frequency of spindle rotation. This setup is modeled in MSC Adams by approximating the cantilever beams as springs with attached fixel masses which in turn are in contact with the workpiece as shown in Figure 5-5. The rigid links which are aligned parallel to the cutting direction are modeled as constraints in this model. The springs are pre-stressed such that they are always compressed thus constantly applying a force on the workpiece. This system is equivalent to an undamped system under harmonic force excitation and hence, the displacement of the workpiece will now be a function of its mass and the frequency of the harmonic force in addition to the stiffness of the fixels (e.g. cantilever beam) and the maximum amplitude of the contact force. The maximum amplitude *X* of the particular solution of such an undamped system under harmonic force is obtained from Equation 5-2 shown below, where F_0 is the maximum amplitude of the harmonic force, *k* is the stiffness of the springs (in parallel) in the system (cantilever fixels), *m* is the mass of the workpiece and ω is the frequency of the harmonic force [13].

$$F = F_0 \sin(\omega t)$$
$$X = \frac{F_0}{k - m\omega^2} \tag{5-2}$$

For an undamped system under a harmonic force, the phase of the particular solution is same as the phase of the harmonic force only when the ratio of the frequency of the harmonic force to the natural frequency ω_n of the system lies between 0 and 1 as shown in Equation 5-3 [13].

$$0 < \omega / \omega_n < 1 \tag{5-3}$$

But the natural frequency of the current system is a function of the spring constant of the cantilever beam and the mass of the workpiece (ignoring fixel mass). Hence, to cancel the errors induced by the runout, the fixels must move the workpiece in phase with the runout. Therefore, the stiffness of the beam has to be chosen such that the natural frequency of such a system is greater than the frequency of spindle rotation.

Now, to study the behavior of the workpiece-fixels system under a harmonic force, the Adams model is to be analyzed at different spindle speeds ranging from 60000 rpm to 90000 rpm, which is the typical range of spindle speeds for a mesoscale system. The value of the runout in the tool is assumed to be in 0.0012 mm and a nominal value of 25 mN is chosen for the maximum amplitude of the harmonic contact force. It should be noted that the value of runout is chosen as 0.0012 mm since it is the least runout value usually observed in high precision systems (found in the literature) and to verify the model for this low value. The value of the harmonic force is chosen to be same as in the static analysis so that there is consistency with the previous analysis. Using Equation 5-2, the value of the stiffness of the compliant beam required to achieve the chosen runout value at different spindle speeds is calculated and tabulated as shown in Table 5-2. It should be noted that the resulting design values of *k* per fixel depend on the number of fixels and their arrangements, yielding an equivalent *k* value for Equation 5-2.

To validate the performance of the design, the frequency of the contact force in the Adams model is initially set to 60000 rpm and the value of the spring constant is set to the value from Table 5-2 corresponding to the spindle speed and the model is run for 0.5 seconds. For this analysis, a plot for the displacement of the center of mass of the workpiece with respect to time is obtained as shown in Figure 5-6. It is observed from this figure that the system has an initial transient state for a very small duration (order of 0.01 seconds) following which the maximum amplitude of the displacement remains constant. This magnitude of the maximum amplitude is measured from the plot and is found to be 0.0012 mm which is equal to the expected runout value.

To better compare the expected runout value and the displacement of the workpiece, these two quantities were plotted together as shown in Figure 5-7. It can be clearly observed from this figure that the displacement of the workpiece is not equal to the runout value for a small duration (close to 0.01 seconds for this example set of conditions) at the beginning of the process. But after this initial transient period, the displacement of the workpiece is equal to the expected runout value along with always being in phase with one another. Thus, the displacement of the center of mass of the workpiece is made equal to the expected runout by varying the length of the compliant beam to achieve the required stiffness values.

To analyze the workpiece-fixel system at various frequencies, the frequencies of harmonic force were varied from 60000 rpm to 90000 rpm and the Adams model is run for these frequencies. During each of the runs, the spring constant is changed to a corresponding value as obtained from Table 5-2. From the Adams models, it is observed that the systems reach steady state quickly and the values of the maximum amplitude of the displacement are equal to the

expected runout values in the steady state. The displacement and runout values are also in phase with another for each of the systems.

To study the error between the displacement of the center of mass of the workpiece and the expected runout value (0.0012 mm in each case) in the transient state, these parameters are plotted for each of the frequencies as shown in Figure 5-8. As can be seen in this figure, the error between these two parameters varies with the frequency of the harmonic force. Also, the time the system takes to reach a constant value is also dependant on the frequency of the force. For higher values of frequencies, the system reaches steady state more quickly as compared to lower frequencies. Also, the maximum value of this error for all the frequencies is measured to be approximately 0.001 mm. Hence, higher frequencies of spindle rotation are optimal for mMT systems. While not shown in Figure 5-8 due to time scale shown for only 0.02 seconds, all cases converge to a low value of error.

To estimate the physical size of the cantilever beams required to obtain the calculated values of spring constants, the stiffness values from Table 5-2 are used to calculate the corresponding lengths of the beam considering the breadth to be 1.25 mm and the width of the beam to be 0.75 mm. These values have been shown in Table 5-3 and it can be observed from this table that the required lengths are comparable to the footprint of the mMT setup. It can also be observed from this table that since the minimum and maximum stiffness values tabulated in Table 5-2 are nothing but the k_{min} and k_{max} values respectively of this configuration of design 2a, the values for length obtained in Table 5-3 are the corresponding L_{max} and L_{min} values. The ratio r of these L_{min} to L_{max} is calculated to be of the order of 0.8 which from the observations of Section 4.2.4 is the optimum value of r for achieving maximum range of stiffness. It is also observed from the table that the slenderness ratio s (ratio of L_{min} to h) for this configuration is greater than

10, thus satisfying the assumption of the design. It should be noted that different combinations of breadth and width of the beam and length of the beam can be used where the critical aspect is acquiring the desired fixel settings.

These stiffness values can also be obtained for designs 2b and 3 for the appropriate values of the parameters of the designs. To estimate the values of these parameters for design 2b, the same stiffness values as before from Table 5-2 are used to calculate the corresponding widths of the beam considering the fixed length of the beam to be 10 mm and the breadth of the beam to be 1.25 mm. The thickness values have been shown in Table 5-4 and are comparable to the mMT setup. It is observed that, similar to design 2a, the minimum and maximum values of width obtained in Table 5-4 represent h_{min} and h_{max} of the current configuration design 2b. The ratio of these minimum and maximum widths is calculated to be in the order of 0.8 which again is the optimum value of r (from Section 4.2.4). Thus the parameters of the current configuration are the optimum values for design 2b. The slenderness ratio s (ratio of L to h_{max}) in this case is also greater than 10.

Similarly for design 3, the values of the distance of the point of application of force from the fixed ends (x) required to achieve the stiffness values from Table 5-2 are calculated and shown in Table 5-5. To calculate these x values, the fixed length of the compliant beam is considered to be 5 mm, the breadth to be 0.5 mm and the width to be 0.25 mm. It can be observed from Table 5-5 that the values of x obtained are achievable for the particular chosen configuration. Similar to the previous designs, the ratio r (ratio of x_{min} to x_{max}) is same as the optimum value of 0.8 and the slenderness ratio s (ratio of L to h) is also greater than 10. Hence, by performing dynamic analysis on the fixel-workpiece system it is established that runout

compensation is achievable using variable stiffness fixels (of designs 2a, 2b or 3) for different frequencies of the spindle rotation.

5.3 Compensation for Transient Dynamics

As observed in the previous section, under the influence of harmonic force, the maximum displacement of the workpiece varies initially before reaching a constant value. This transient state exists for a very short duration but its effect on accuracy depends on the feed rate of the process. For small feed rates, the length of the workpiece machined in this small duration will not create excess inaccuracies. But in the case of high feed rates, these inaccuracies cannot be negligible. If the effects of the transient dynamics are not negligible, to counter this variation it is proposed that sacrificial material be used for the initial duration of the process. The sacrificial material is to be obtained by using a longer (in case of milling) or thicker (in case of drilling) workpiece and discarding the excess length/thickness after the completion of the operation.

In the determination of the appropriate fixel stiffness, the workpiece mass value will need to include the mass of the sacrificial material in the calculation of the length of the cantilever beam corresponding to a runout value.

Table 5-1. Overview of the runout and length values for various trials obtained from the FE Analysis

Runout values in mm	Runout values obtained from the ProE model	Length of the cantilever beam, *L* in mm
0.1488	0.15255	9.999
0.1354	0.13903	9.962
0.1182	0.11989	9.742
0.0957	0.09795	9.307
0.0813	0.08245	9.053
0.0645	0.06642	8.628
0.0492	0.05142	8.137
0.0381	0.03647	7.999

Table 5-2. Calculation of the stiffness values corresponding to different spindle speeds

Spindle rotation speed in rpm	Maximum amplitude of the contact force in mN	Expected runout value in mm	Calculated stiffness values in N/mm
60000	25	0.0012	29.645
66000	25	0.0012	33.683
72000	25	0.0012	38.106
78000	25	0.0012	42.913
84000	25	0.0012	48.105
90000	25	0.0012	53.681

Table 5-3. Calculation of the lengths of the compliant beams corresponding to the beam stiffness values for Design 2a

Calculated stiffness values in N/mm	Breadth of the compliant beam in mm	Width of the compliant beam in mm	Length of the compliant beam in mm
29.645	1.25	0.75	9.725
33.683	1.25	0.75	9.320
38.106	1.25	0.75	8.945
42.913	1.25	0.75	8.597
48.105	1.25	0.75	8.276
53.681	1.25	0.75	7.979

Table 5-4. Calculation of the widths of the compliant beams corresponding to the beam stiffness values for Design 2b

Calculated stiffness values in N/mm	Breadth of the compliant beam in mm	Length of the compliant beam in mm	Width of the compliant beam in mm
29.645	1.25	10.00	0.771
33.683	1.25	10.00	0.805
38.106	1.25	10.00	0.838
42.913	1.25	10.00	0.872
48.105	1.25	10.00	0.906
53.681	1.25	10.00	0.934

Table 5-5. Calculation of distance of point of application of force from the fixed end of the compliant beams corresponding to the beam stiffness values for Design 3

Calculated stiffness values in N/mm	Length of the compliant beam in mm	Breadth of the compliant beam in mm	Width of the compliant beam in mm	Value of x in mm
29.645	5.00	0.5	0.25	1.387
33.683	5.00	0.5	0.25	1.319
38.106	5.00	0.5	0.25	1.257
42.913	5.00	0.5	0.25	1.200
48.105	5.00	0.5	0.25	1.149
53.681	5.00	0.5	0.25	1.101

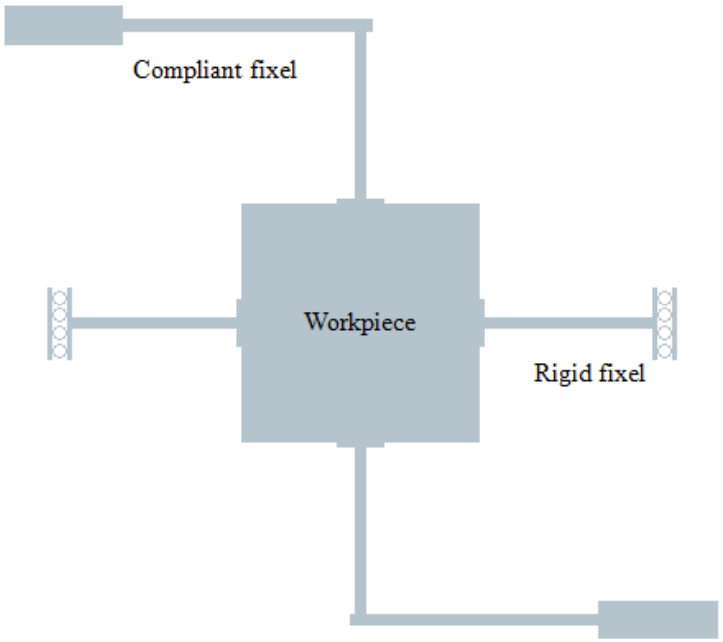

Figure 5-1. ProE model for fixel– workpiece configuration for a milling operation with two compliant fixels and two rigid fixels

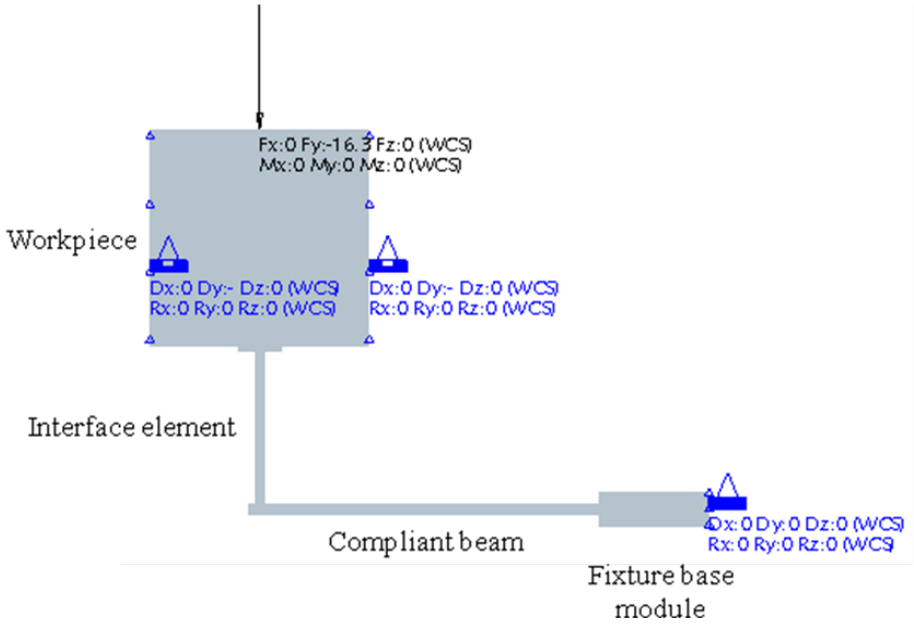

Figure 5-2. ProE model for single fixel – workpiece configuration

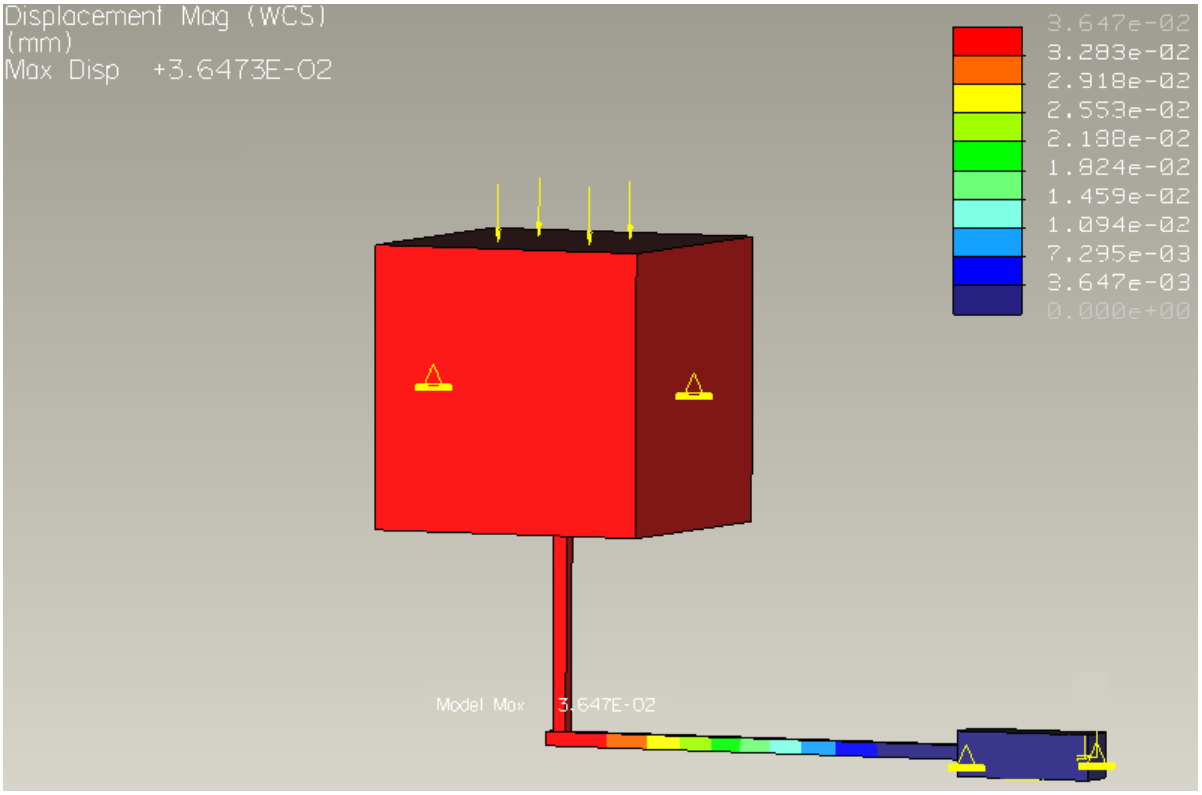

Figure 5-3. FE Analysis to calculate the maximum displacement of the compliant beam

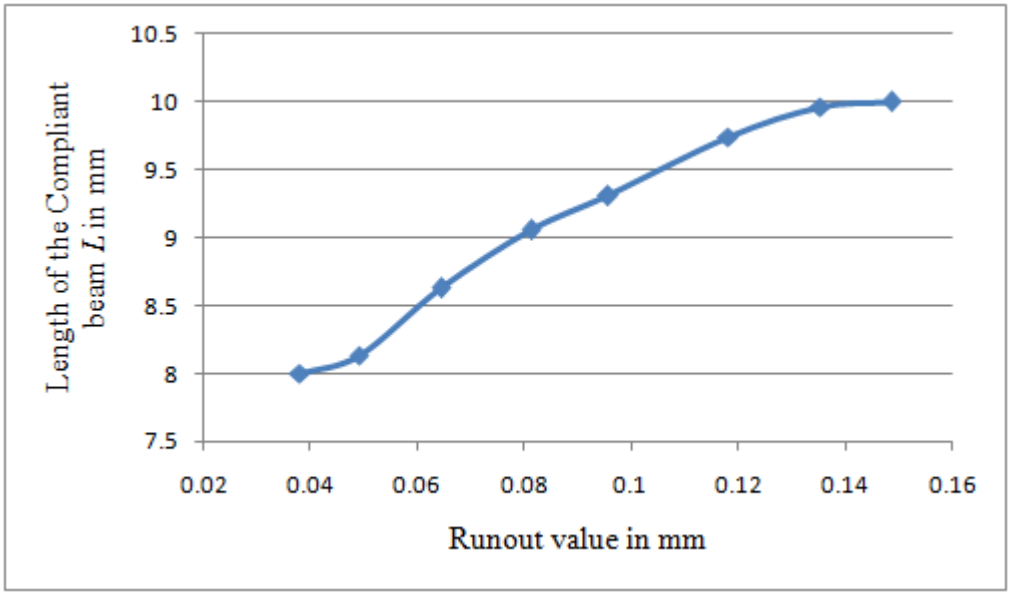

Figure 5-4. Variation of length of the cantilever beam for corresponding runout values

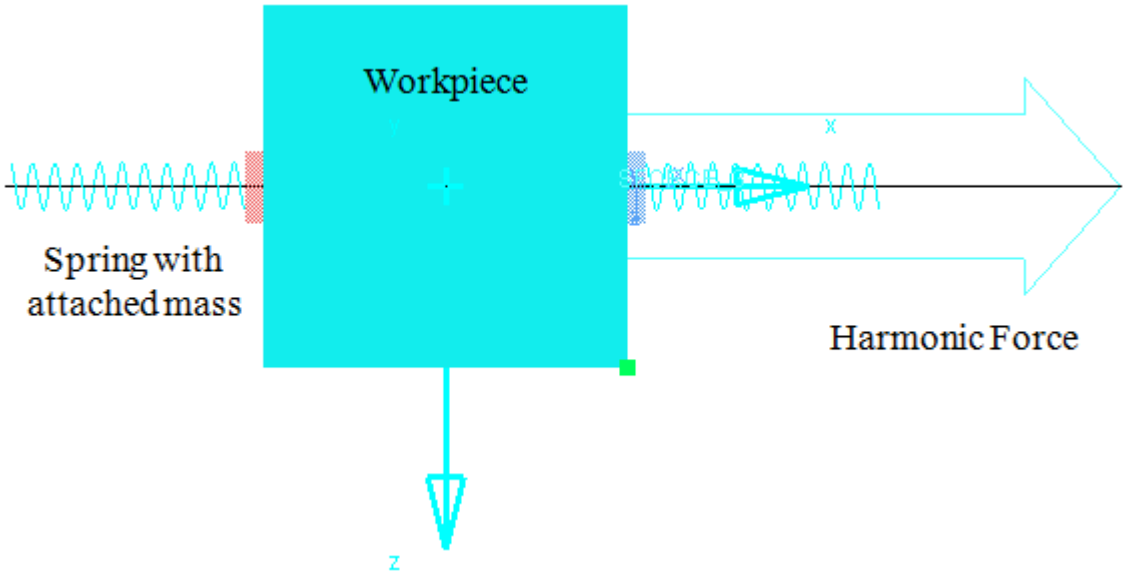

Figure 5-5. MSC Adams model for the two fixels-workpiece configuration

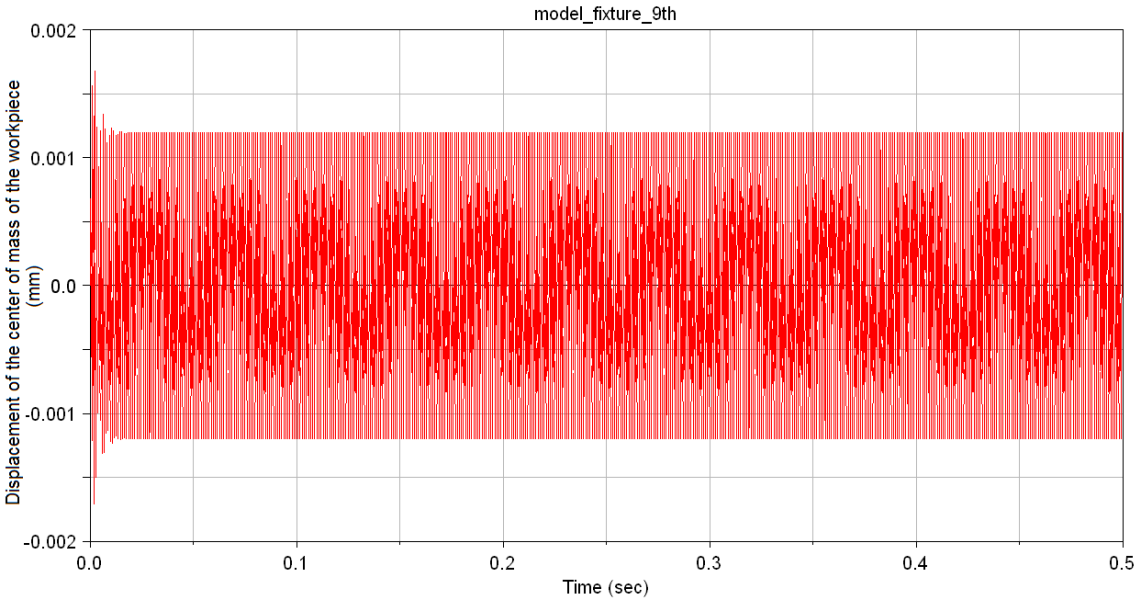

Figure 5-6. Plot showing the Displacement of the center of mass of the workpiece with respect to time where the frequency of the harmonic force is 60000 rpm

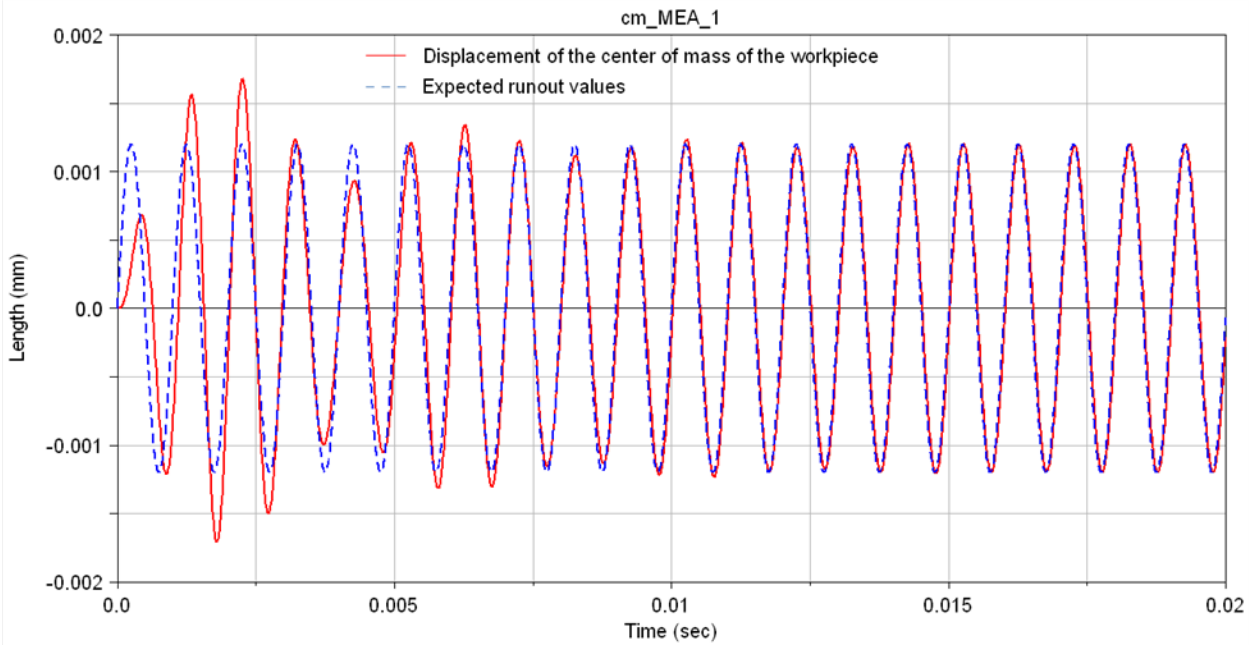

Figure 5-7. Comparison of the displacement of the center of mass of the workpiece and the expected runout values for a frequency of 60000 rpm

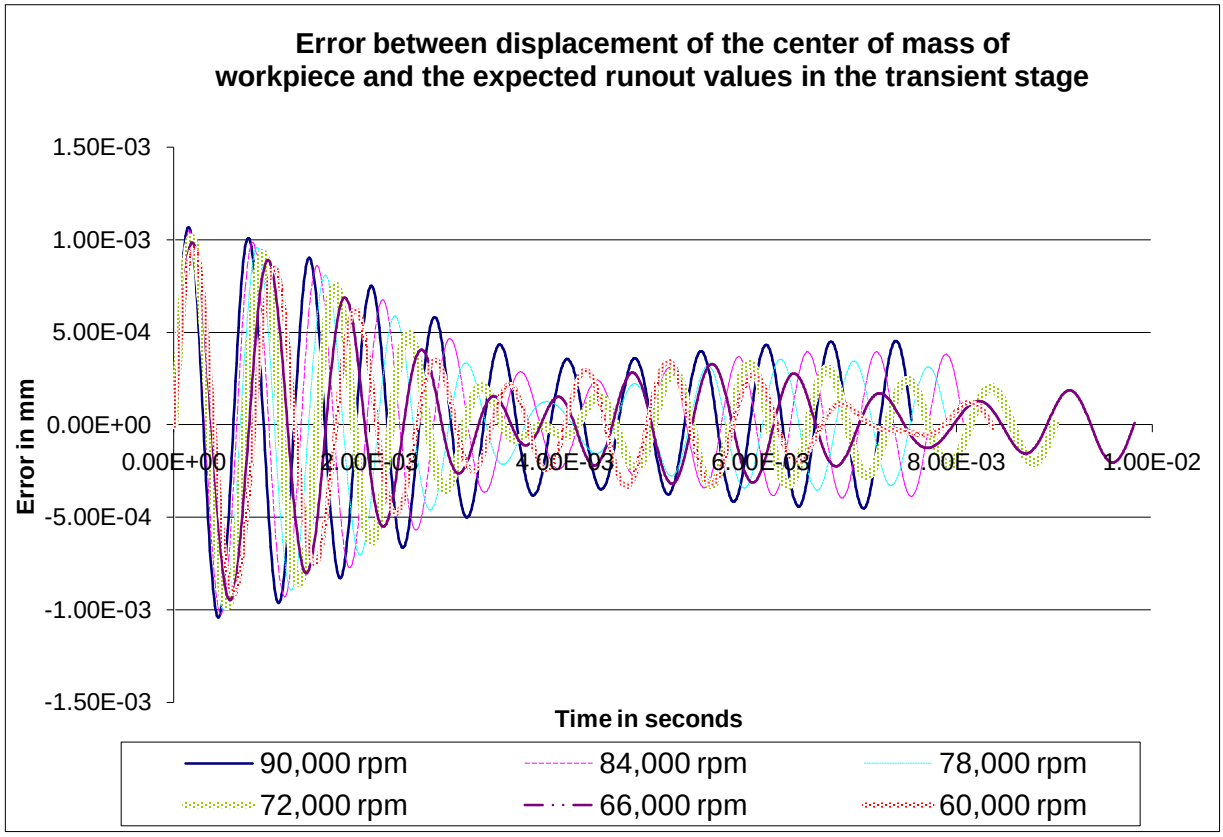

Figure 5-8. Plot showing the error between the displacement of the center of mass of the workpiece and the expected runout values in the transient stage

CHAPTER 6
DISCUSSION AND CONCLUSIONS

6.1 Conclusions

The motivation for investigating the fixel designs presented in this thesis is driven by the conjecture that through the provision of mechanically adaptable stiffness characteristics in passive/active fixturing one can potentially improve the dynamic response of the workpiece during manufacturing of micron features. This study has provided the theoretical modeling of four such fixel designs and a comparison of what stiffness trends one may extract from their design.

It is observed that four-bar mechanism type fixel offers greater versatility in that it exhibits two mechanical variables for making adjustments. But this adds to the complexity of the design by requiring twice as many actuators for controlling these variables. However, the results indicate that by controlling one of the parameters, the fixel can still be tuned to control the dynamic behavior. In addition, the trends observed in the stiffness as a function of the mechanical variables exhibit local minimums.

For the beam type fixels, Designs 2a and 3 offer continuous adaptability fixel stiffness while the Design 2b uses incremental adjustments in changing its stiffness. For these three designs, it was found that similar trends occurred in terms of k versus available range of input variable. Additionally, the lower bound on the slenderness ratio contributed to an amplification of the rate of change in k with respect to change in input variable, as well as on the range of k. Design 2a and 2b yield the greatest of all values for range of k while Design 2b yields the greatest value for the average slope of k. But since design 2b is potentially hampered by the discrete nature of its design, its practical application will be difficult. Hence, considering both

the stiffness characteristics and ease of application, Design 2a is the best among the fixel designs.

To analyze the performance of the proposed designs, one of the designs (Design 2a) is analyzed by implementing it in an end milling mesoscale machine tool system where the tool has runout along the direction of the fixels. The fixel-workpiece system was initially modeled in ProE and a static analysis was performed, from which it was established that runout compensation can be achieved by adjusting the length of the compliant beam to obtain beam deflection equal to the runout error. To simulate a mesoscale tool system, a MSC Adams model was developed and analyzed under the influence of a harmonic force and other typical mesoscale system operation parameters. It was observed that runout compensation can be achieved in this case as well, but the length of the compliant beam was now a function of the frequency of the spindle rotation and the mass of the workpiece in addition to the stiffness of the compliant beam.

To conclude, four different fixel designs have been presented that exhibit the mechanical adaptability of their stiffness characteristics and analysis has been performed on one of the designs to prove the implementation of the design concept for fixturing for mesoscale manufacturing. A provisional patent for the designs proposed in this thesis has been obtained.

6.2 Directions for Future Research

For further research, these designs need to be tested experimentally to further quantify their ability to control the dynamic response of the tool-workpiece-fixture interface. In addition, implementation issues in terms of actuators and sensors and their real-time control and effects of friction in the fixture-workpiece platform (support surface) need further study. It should be noted that the research in this thesis focuses on application of the fixel designs within the fixturing system by using two or four fixels. The determination of the specific number and optimal

locations of the fixels required, which is workpiece and process dependent, has been left for future work. Also, the determination of the optimal contact force has been left for future work.

It has been observed from the analysis of the fixel designs that the workpiece-fixture system under the influence a harmonic force experiences a transient period before reaching the steady state. The effect of this transient nature of the displacement of the workpiece on the accuracy of the process will be dependent on the feed rate values. A methodology to reduce the duration of the transient state needs to be developed which will be done during further research. Also, the sensitivity of the results of the analysis to variations in the mass of the workpiece has not been studied. This will be studied in future work to quantify its significance on part accuracy for such scenarios in which material is being removed.

REFERENCES

[1] S. W. Lee, R. Mayor and J. Ni, “Dynamic analysis of a mesoscale machine tool,” Journal of Manufacturing Science and Engineering, 128 (1), 194 – 203, 2006.

[2] A.H. Honegger, S.G. Kapoor and R.E. DeVor, “A hybrid methodology for kinematic calibration of micro/meso-scale machine tools (mMTs),” ASME Journal of Manufacturing Science and Engineering, 128 (2), 13 – 18, 2006.

[3] H. Li, X. Lai, C. Li, Z. Lin, J. Miao, J. Ni, “Development of meso-scale milling machine tool and its performance analysis,” in the Chinese Journal of Mechanical Engineering, 42 (11), 162 – 167, 2006.

[4] J. Bronson, G. Wiens, J. Palmer and J.R. Meyer, “Feasibility study of mechanically adaptive microfabrication process tooling and fixturing,” 1st International Conference on Micromanufacuring, ICOMM 2006, University of Illinois at Urbana-Champaign, IL, 2006.

[5] G.J. Wiens, R.M. Wagner, A. Valdes and J.R. Bronson, "Mechanically-adaptive fixture element for directional control of contact interface forces," International Conference on Micro-Manufacturing 2007, Clemson University, SC, 2007.

[6] M.L. Culpepper and S. Kim, “Six-axis reconfigurable nanomanipulator systems for positioning in nano-scale manufacturing and research,” International Symposium on Nano-Manufacturing, ISNM 2004, Daejeon, Korea, 2004.

[7] U.A. Tol, G.J. Wiens and J. Schueller, “Mechanical adaptability of active fixturing system,” submitted for refereed journal publication, 2009.

[8] B.S. El-Khasawneh and P.M. Ferreira, “Computation of stiffness and stiffness bounds for parallel link manipulators”, International Journal of Machine Tools & Manufacture, 39 (1), 321 – 341, 1999.

[9] G.J. Wiens and D.S. Hardage, “Structural dynamics and system identification of parallel kinematic mechanisms,” in Proceedings of the International Design Engineering Technical Conferences, DETC2006, 2006, pp. 10.

[10] W.F. Riley, L.D. Sturges and D.H. Morris, Mechanics of materials, John Wiley & Sons, New York, NY, pp. 475 – 484, 1999.

[11] L.L. Howell, Compliant mechanisms, John Wiley & Sons, New York, NY, 2001.

[12] D.L.Martin and R.O.Wilcox, “Spindle runout effects on postional accuracy,” in the University of Wisconsin Symposium on Small Hole Techonolgy, Palm Springs, California, 1990.

[13] S.S.Rao, Mechanical mibrations, Pearson Eduaction, Inc., New Jersey, NJ, pp 221 – 225, 2004.

BIOGRAPHICAL SKETCH

Koustubh Rao was born in India, in 1984. He received his bachelor's degree in mechanical engineering from the Indian Institute of Technology Guwahati, Guwahati, India in May 2006.

Mr. Rao will have received his Master of Science degree in mechanical engineering from University of Florida in August 2009. At University of Florida, he worked in the Space Automation and Manufacturing Mechanisms Laboratory in the Department of Mechanical and Aerospace Engineering under the guidance of Dr. G. Wiens.